Master Thesis

DEVELOPMENT OF A TABLETOP ELECTRO-SPECTROMETER FOLLOWING THE MAC-E-FILTER PRINCIPLE

vorgelegt von
Maik Schneider

Institut für Kernphysik

- January 2018 -

Erster Gutacher: Prof. Dr. C. Weinheimer
Zweiter Gutachter: PD. Dr. C. Klein-Bösing

Plagiatserklärung des Studierenden

Hiermit versichere ich, dass die vorliegende Arbeit über

Development of a tabletop electrospectrometer following the MAC-E-Filter principle

selbstständig verfasst worden ist, dass keine anderen Quellen und Hilfsmittel als die angegebenen benutzt worden sind und dass die Stellen der Arbeit, die anderen Werken – auch elektronischen Medien – dem Wortlaut oder Sinn nach entnommen wurden, auf jeden Fall unter Angabe der Quelle als Entlehnung kenntlich gemacht worden sind.

_____

Münster, 18.01.2018

Ich erkläre mich mit einem Abgleich der Arbeit mit anderen Texten zwecks Auffindung von Übereinstimmungen sowie mit einer zu diesem Zweck vorzunehmenden Speicherung der Arbeit in eine Datenbank einverstanden.

_____

Münster, 18.01.2018

Contents

1 Introduction

The neutrino is part of the standard model as a massless, only weakly interacting particle, but since the observation of neutrino oscillation in 1998 [SK98], that requires a non-zero neutrino mass, the search for the mass of the neutrinos received renewed interest, in a lot of different experiments. Being relevant not only in particle physics, but also astrophysics as well as cosmology, it is a window to physics beyond the standard model.

Many limits on the neutrino mass are model-dependent, stemming from astrophysical experiments, especially from measurements of the cosmic microwave background. Which is why a model independent kinematic search for the neutrino mass is important. Already the experiments in Mainz and Troitsk were conducted on this basis. Through these results a current limit on the mass of the electron anti-neutrino of around 2 eV was set [Kra$^+$13, Ase$^+$11]. The KATRIN experiment, scheduled to start operation in 2018, aims for an improved sensitivity of 0.2 eV (90% C.L.).

These experiments all use the MAC-E-Filter principle, in spectrometers ranging from a few meters length and diameter, to above 23 m length and nearly 10 m diameter for the KATRIN main spectrometer.

In this thesis a tabletop spectrometer following the same principle is designed, optimized and tested. It is investigated if the MAC-E-Filter principle can be realized in such a small space, while maintaining a reasonable energy resolution in the process.

In chapter 2 a quick overview of the history of neutrino physics and the properties of the neutrino will be given. Chapter 3 introduces the theory behind the MAC-E-Filter principle. Then the simulations performed to improve the design of the tabletop spectrometer are shown in chapter 4, which was then build in the laboratory in Münster shown in chapter 4. Chapter 6 and 7 describe the measurements conducted with the spectrometer and their analysis, respectively. In the end chapter 8 contains a summary of the thesis and an outlook on possible improvements.

2 Neutrino physics

2.1 Beta-Decay

Contrary to particles produced in α- and γ-decay the electrons produced in β-decays show a continuous energy and momentum spectrum. At first this led to the assumption that conservation laws could be violated in β-decay.
In 1930 Wolfgang Pauli postulated the existence of the neutrino, that serves to take away the missing momentum and energy. Treating the β-decay as a 3-body decay,

$$n \to p + \overline{\nu}_e + e^-. \tag{2.1}$$

Because the neutrino carries no electric charge and the weak interaction has only a short range, it was already clear that detecting neutrinos in an experiment would be very difficult. To compensate for the weak interaction either a huge detector-mass or a strong neutrino source would be necessary. Both weren't available in the 1930's. It took until 1956, when the Cowan-Reines neutrino experiment [RC59] discovered the neutrino via the inverse β-decay,

$$p + \nu_e \to n + e^-. \tag{2.2}$$

2.2 Neutrino Oscillation

For a long time the neutrino was assumed to have zero mass, and in the standard model the neutrinos are thought of as massless particles as well. But in experiments measuring the neutrino flux originating from the sun, only 1/3 of the expected neutrino flux was observed. Which came to be known as the solar neutrino problem.
One possibility to solve this problem is the theory of neutrino oscillation, which assumes that neutrinos have mass eigenstates $\nu_i (i = 1, 2, 3)$. This means that neutrinos have mass and can change their flavor state while moving, if these eigenstates are not identical to the flavor eigenstates $\nu_\alpha (\alpha = e, \mu, \tau)$.

Now the flavor eigenstates can be written as a superposition of the mass eigenstate,

$$|\nu_\alpha\rangle = \sum_i U_{\alpha i} |\nu_i\rangle, \tag{2.3}$$

using a 3×3 unitary mixing matrix. For the neutrino mixing this matrix is called Pontecorvo-Maki-Nakagawa-Sakata(PMNS) matrix,

$$U = \begin{pmatrix} c_{12}c_{13} & s_{12}c_{13} & s_{13}e^{-i\delta} \\ -s_{12}c_{23} - c_{12}s_{23}s_{13}e^{i\delta} & c_{12}c_{23} - s_{12}s_{23}s_{13}e^{i\delta} & s_{23}c_{13} \\ s_{12}s_{23} - c_{12}s_{23}s_{13}e^{i\delta} & -c_{12}s_{23} - s_{12}c_{23}s_{13}e^{i\delta} & c_{23}c_{13} \end{pmatrix}, \tag{2.4}$$

where c_{ij} and s_{ij} are the cosine and sine of the mixing angle θ_{ij} respectively. The phase δ accounts for a possible CP-violation, which has not been observed yet.

To understand the difference of the observed abundance of solar neutrinos, it is necessary to understand the development of a mass eigenstate with time. Hence the Schrödinger equation is applied, using $\hbar = c = 1$:

$$|\nu_i(t)\rangle = e^{iE_i t}|\nu_i\rangle, \tag{2.5}$$

where the neutrino energy E_i is

$$E_i = \sqrt{p_i^2c^2 + m_i^2c^4} \approx E + \frac{m_i^2c^4}{2E}, \quad \text{if} \quad p \gg m_i. \tag{2.6}$$

Now expressing equation 2.5 as a function of the traveled distance $L := ct$

$$|\nu_i(L)\rangle = e^{im_i^2 L/2E}|\nu_i\rangle, \tag{2.7}$$

gives the probability that a flavor eigenstate is transformed:

$$P_{\alpha\to\beta} = |\langle\nu_\beta(L)|\nu_\alpha\rangle|^2 = \left|\sum_i U_{\alpha i}U^*_{\beta i}e^{im_i^2 L/2E}\right|^2. \tag{2.8}$$

This can be expanded to

$$\begin{aligned} P_{\alpha\to\beta} = \delta_{\alpha\beta} &- 4\sum_{i>j} Re(U_{\alpha i}U^*_{\beta i}U^*_{\alpha j}U_{\beta j}) \sin^2\left(\frac{\Delta m_{ij}^2 L}{4E}\right) \\ &+ 2\sum_{i>j} Im(U_{\alpha i}U^*_{\beta i}U^*_{\alpha j}U_{\beta j}) \sin\left(\frac{\Delta m_{ij}^2 L}{2E}\right), \end{aligned}$$

with $\Delta m_{ij}^2 = m_i^2 - m_j^2$.

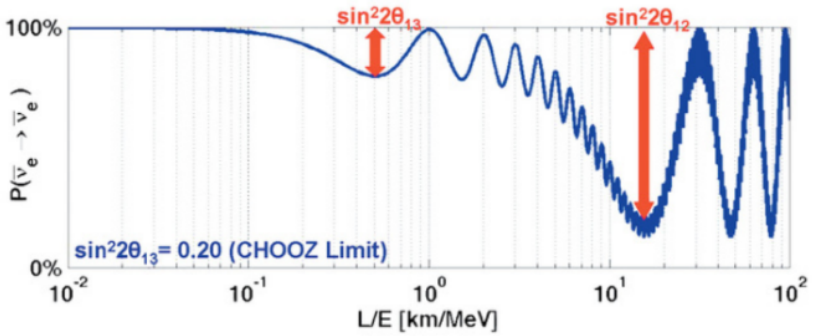

Figure 2.1: **Transition probability for the $\nu_e \to \nu_e$ process:** For small L to E proportions, the probability to remain in the initial flavor eigenstate is nearly 1. As the L/E value rises, the probability starts oscillating and transition to other flavor eigenstates becomes allowed [Kat06].

In the case of atmospheric neutrino oscillation ($\nu_\mu \to \nu_\tau$) and solar neutrino oscillation ($\nu_e \to \nu_\mu$) mainly two neutrino flavours are relevant and can be described by only one angle θ and one mass difference $\Delta m^2 = |m_1^2 - m_2^2|$ leading to the simplified equation

$$P_{\alpha\to\beta} = \sin^2(2\theta)\sin^2\left(\frac{\Delta m^2 L}{4E}\right). \tag{2.9}$$

The Super-Kamiokande experiment gave first evidence for neutrino oscillation in 1998. Located 1000 m under mount Kamioka, Japan, a water Cherenkov detector, filled with $50,000$ tons of ultra-pure water, detected incoming neutrinos. By interaction with the electrons and nuclei of the water atoms, the neutrinos produce charged particles faster than the speed of light in the medium, hence producing cherenkov radiation, that was picked up by photomultiplier tubes inside the tank. Being the first experiment to be able to distinguish between electron neutrino and muon neutrino events, the ratio between the two event types could be determined and compared to Monte Carlo Simulation. This led to the evidence of neutrino oscillation[SK98].

Apart from the proof of neutrino oscillation, the Super-Kamiokande experiment could also measure the parameters $\Delta m^2_{32} = (2.43 \pm 0.13)10^{-3}$ eV^2 and $\theta_{23} = 45° \pm 7.1°$. The mass difference $\Delta m^2_{12} = (2.1^{+0.20}_{-0.21})10^{-5}$ eV^2 and the mixing angle $\theta_{12} = 34.06°^{+1.16°}_{-0.84°}$, were subsequently determined by the SNO and Kamland experiments, observing solar neutrinos. The remaining mixing angle could be determined through measurements of experiments like Daya Bay, Double Chooz and RENO to $\sin^2(2\theta_{13}) = 0.092 \pm 0.017$.

2.3 Search for the neutrino mass

Even though the mentioned experiments were a success in their own right, they were only able to measure squared mass differences, but not the absolute mass of the neutrinos themselves. To do this there are 3 different types of experiments being conducted right now.

- Cosmological and Astrophysical experiments like WMAP, PLANCK and the Hubble Space Telescope are sensitive to the sum of the three neutrino masses. Neutrino properties are here extracted from data about cosmic structure formation. These measurements led to strong upper limits on the sum of the neutrino masses, one of the best constraints amounts to $\sum m_\nu < 0.29$ eV [RS12].
  The downside to this type of experiments are a strong model dependence of this type of interpretation.

- A more direct approach is taken by experiments looking for the neutrinoless double β decay. For this process to happen the neutrino needs to be a Majorana particle (it is its own anti-particle).
  In this process two β decays happen simultaneously, while the neutrino that is emitted from one nucleon is absorbed by the other. The decay rate of this process is given by

  $$\Gamma = G|M|^2|m_{ee}|^2,$$

  which depends on the coherent sum of the neutrino mass eigenstates

  $$m_{ee}^2 = \left|\sum_i U_{ei}^2 m(\nu_i)\right|.$$

  The GERDA collaboration found a lower limit of $2.1 \cdot 10^{25}$ years for the half life of this decay [Ago$^+$13].

- Measuring the spectrum of the β-decay provides a way to directly measure the neutrino mass. This approach is entirely based on relativistic kinematic and therefore model-independent.
  Since the neutrino mass is nonzero, it will at least take the energy corresponding to its rest mass from the total decay energy. This means that the upper limit of the electron energy is directly connected to the electron neutrino mass

$$m^2(\nu_e) = \sum_i |U_{ei}|^2 m(\nu_i)^2.$$

  Applying Fermi's Golden Rule and neglecting the recoil energy of the nucleus, because of its much higher mass and the final state distribution of the daughter molecule, the electron energy spectrum is given by:

$$\frac{d\dot{N}}{dE} = R(E)\sqrt{(E_0 - E) - m_{\bar{\nu}_e}^2 c^4}\,\theta(E_0 - E - m_{\bar{\nu}_e}c^2).$$

$$R(E) = \frac{G_F^2}{2\pi^3\hbar^7}\cos^2(\theta_C)|M|^2 F(Z,E)p(E + m_e c^2)(E_0 - E),$$

  with E the energy of the electron, E_0 the Endpoint energy of the β-spectrum, G_F the Fermi constant, θ_C the Cabbibo-angle, M the nuclear matrix element, Z the atomic number of the daughter nucleus and m_e the mass of the electron.
  In figure 2.2 the effect of the neutrino mass on the tritium spectrum is shown. Not only the endpoint but the whole shape of the spectrum is influenced by the neutrino mass. It also shows that only a small fraction of all electrons is located in the endpoint region. For tritium about $2 \cdot 10^{-13}$ of all electrons have energies in the interval of the last 1 eV.

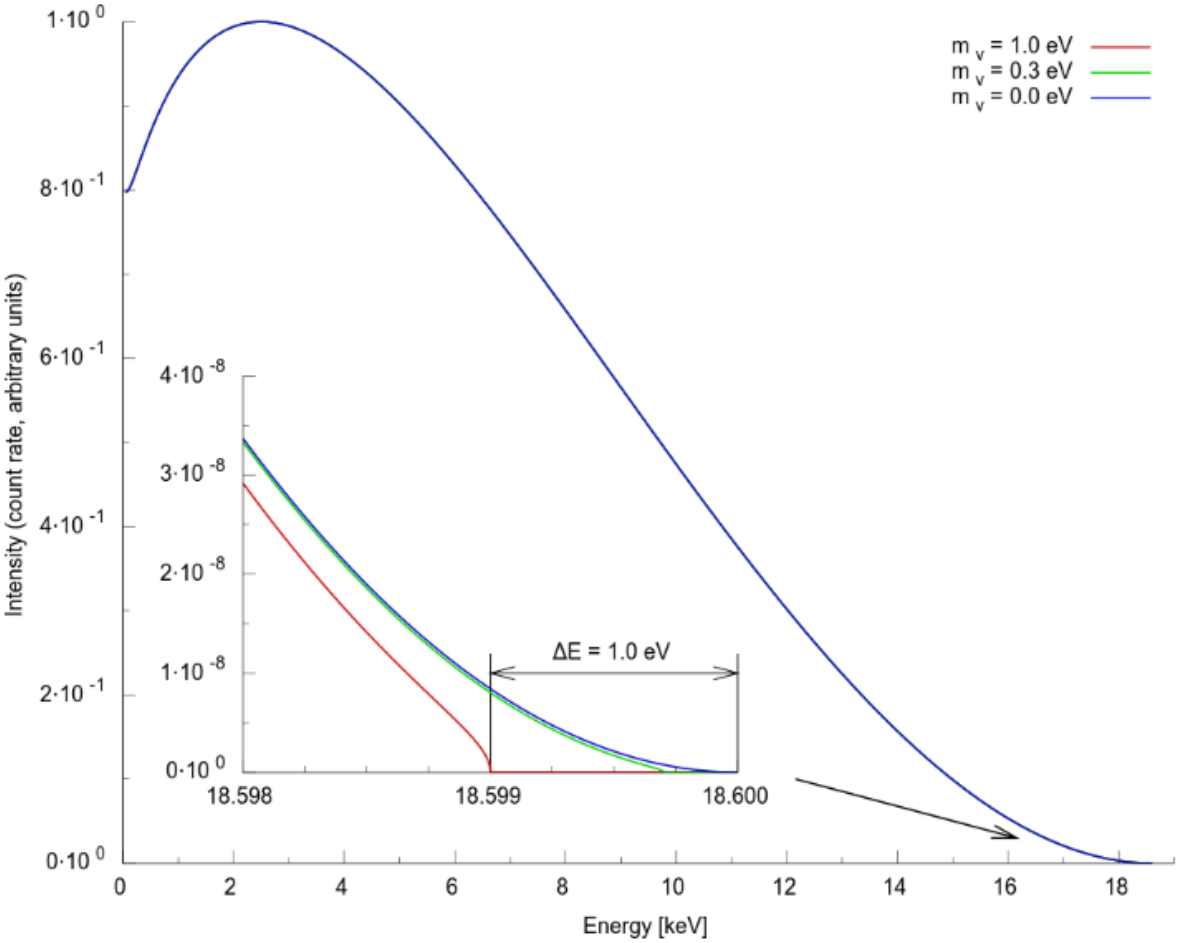

Figure 2.2: Energy spectrum of the tritium β-decay in dependence of 3 different neutrino masses. The inset shows that not only the endpoint but also the shape is influenced by the neutrino mass [Beh12].

3 MAC-E-Filter principle

The **M**agnetic **A**diabatic **C**ollimation combined with an **E**lectrostatic (**MAC-E**) filter technique combines electric retardation and an inhomogeneous magnetic guiding field to measure the kinetic energy of a charged particle. This type of spectrometer offers a high energy resolution and angular acceptance. Both features are useful for an analysis near the endpoint of a β-emitter with low statistics.
Since electrons near the endpoint of the tritium β-spectrum at ≈ 18.6 keV and also conversion electrons from $^{83\mathrm{m}}$Kr β-decay ($E = 17.824$ keV) that are used for the measurements in this thesis only have a small Lorentz factor,

$$\gamma = \frac{1}{\sqrt{1 - \frac{v^2}{c^2}}} \approx 1.04,$$

the following discussion will be completely non-relativistic.

3.1 Working principle

Since in an electrostatic spectrometer only the component of the electron momentum parallel to the electric field lines can be analysed, a MAC-E-Filter uses magnetic collimation to rotate the momentum vector of the particles into this direction. For this purpose, the electron moves from a strong magnetic field at the entrance of the spectrometer to a low magnetic field, whose field lines are parallel to the electric field lines in the centre of the spectrometer, the so called analysing plane, see figure 3.1.
An electron emitted into the MAC-E-filter with a starting energy E_{start}, under an angle $\theta \angle(\vec{B}, \vec{p})$ between its momentum $\vec{p}$ and the magnetic field $\vec{B}$, performs a cyclotron motion around the field line. Perpendicular to the field line the electron possesses an energy of

$$E_\perp = E_{start} \sin^2(\theta),$$

thus creating an orbital magnetic moment

$$\mu = \frac{q}{2m}\vec{l} = \frac{E_\perp}{B},$$

where $\vec{l}$ is the angular momentum. Through the gradient of the magnetic field a force parallel to the field lines is applied and since the energy is conserved in a static magnetic field the energy perpendicular to the field lines is converted into parallel energy.

While moving through the spectrometer the particle performs a cyclotron motion around the magnetic field lines. If the change of the magnetic field in one cyclotron loop is sufficiently small, i.e.

$$\left|\frac{1}{B}\frac{dB}{dt}\right| \ll \omega_{cyc} = \frac{qB}{m}, \tag{3.1}$$

the motion is adiabatic and the magnetic moment μ is a constant of motion. This allows to tell how much of the initial perpendicular energy $E_{\perp,i}$ is transformed into parallel energy, between the initial magnetic field B_i and the minimal magnetic field in the analysing plane B_{ana},

$$E_{\perp,ana} = E_{\perp,i}\frac{B_{ana}}{B_i}. \tag{3.2}$$

3.2 Energy resolution and transmission function

Assuming the Voltage in the analysing plane U_0 is exactly known, the energy resolution of an ideal MAC-E-filter is given by the maximal amount of remaining transversal kinetic energy, which can be calculated using equation (3.2),

$$E_{\perp,max} = E_{start,max}\frac{B_{ana}}{B_{max}} = \Delta E. \tag{3.3}$$

In an actual laboratory setup, the resolution is further reduced by experimental imperfections like inhomogeneities of the electric and magnetic fields in the analysing plane or fluctuations of the retardation voltage.
Only particles with

$$E_{\parallel,ana} - qU_0 > 0, \tag{3.4}$$

can pass the spectrometer. This shows that the spectrometer acts as a high pass filter.Using equation (3.2) one can also determine the change of the angle θ between two points in the spectrometer to

$$\sin^2\theta_f = \frac{B_f}{B_i}\sin^2\theta_i.$$

The transmission condition for a particle with energy $E_{kin} \approx qU_0$, can now be expressed with the angle θ_s, it has at its starting point.

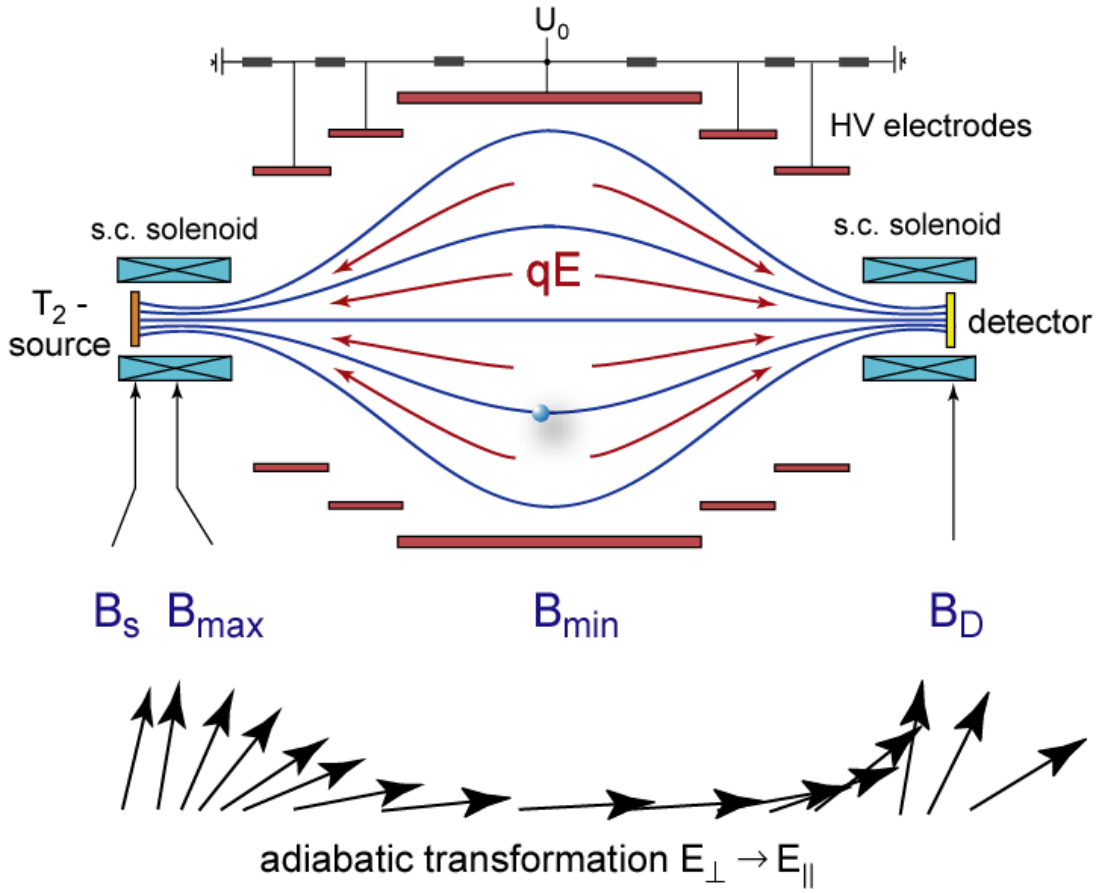

Figure 3.1: Sketch of a cross section of a MAC-E-Filter setup. Shown in red are the electrodes, with the retardation voltage U_0, enveloping the magnetic flux (blue lines). On both sides of the electrodes solenoids produce the magnetic guiding field. On the bottom the adiabatic transformation of the momentum vector parallel to the magnetic field line is shown. Source and Detector are placed in the maximal magnetic field inside the solenoids.

$$
\begin{aligned}
0 &< E_{\parallel,ana} - qU_0 \\
&= E_{kin} - E_{\perp,ana} - qU_0 \\
&= E_{kin}(1 - \sin^2\theta_{ana}) - qU_0 \\
&= E_{kin}(1 - \frac{B_{ana}}{B_s}\sin^2\theta_s) - qU_0.
\end{aligned}
$$

Solving the equation for θ_s shows which starting angles are transmitted through the spectrometer, depending on the kinetic energy of the particle and the analyzing Voltage U_0.

$$
\theta_s < \theta_s^{max}(E_{kin}, qU_0) = \arcsin\left(\sqrt{\frac{E_{kin} - qU_0}{E_{kin}}\frac{B_s}{B_{ana}}}\right).
$$

This reduces the theoretical angular acceptance of 2π and the solid angle $\Delta\Omega$ accepted by the filter is connected to the maximal starting angle through

$$
\frac{\Delta\Omega}{2\pi} = 1 - \cos(\theta_s^{max}). \tag{3.5}
$$

By using the relation $\cos(\arcsin(\sqrt{x})) = \sqrt{1-x}$ the transmission function can be written as

$$
T(E_{start}, U_0) = \begin{cases} 0, & \text{for} \quad E_{start} < qU_0 \\ 1 - \sqrt{1 - \frac{E_{start} - qU_0}{E_{start}}\frac{B_{max}}{B_{ana}}}, & \text{for} \quad qU_0 < E_{start} < qU_0 + \Delta E \\ 1, & \text{for} \quad qU_0 + \Delta E < E_{start}. \end{cases} \tag{3.6}
$$

Equation 3.6 shows that the MAC-E-Filter works as an integrating high pass filter and is visualized in figure 3.2.

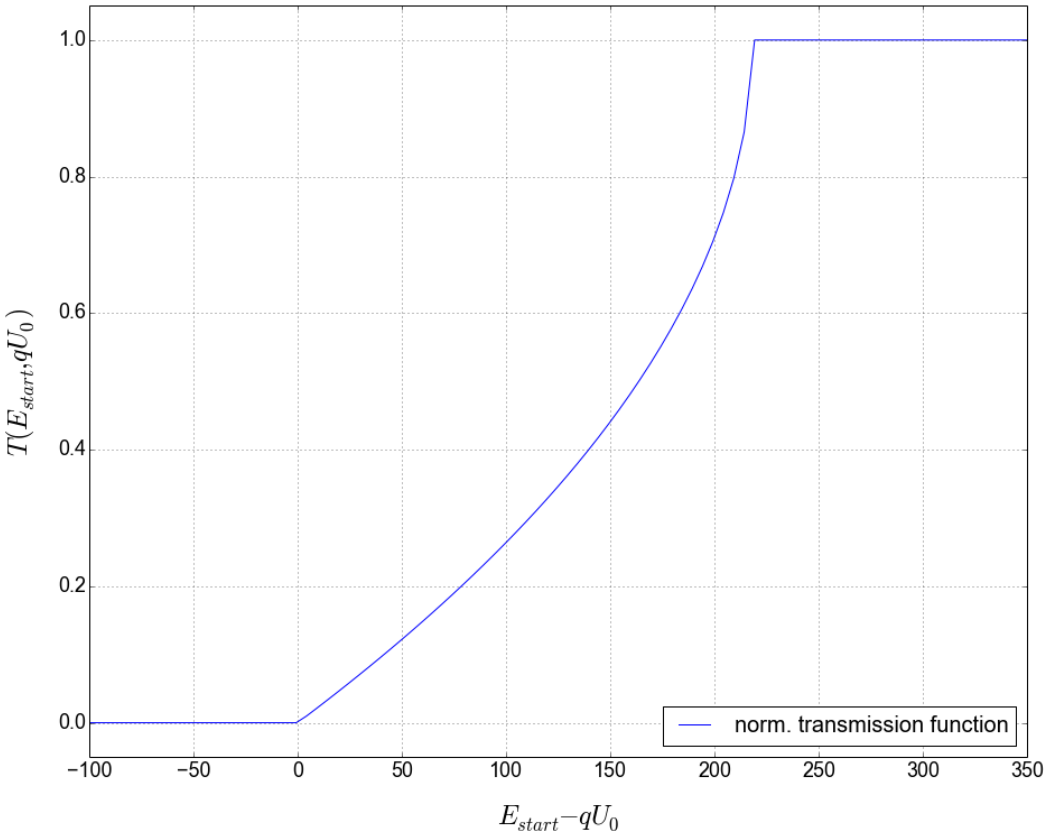

Figure 3.2: Analytical transmission function of a MAC-E-filter, for an isotropically emitting source. Shown here for the design values of the Katrino experiment of $B_{start} = 0.49$ T and $B_{ana} = 6$ mT. Electrons with high angles to the magnetic field need a higher surplus energy to get transmitted.

4 Simulations

As simulations in this thesis play a substantial role in the design and optimization of a MAC-E-Filter, for a better understanding a short summary of the used software will be given, before the requirements for a tabletop spectrometer and their realization in the simulations are discussed.

4.1 Kassiopeia

The simulations are based on the *Kassiopeia* framework, developed by the **KATRIN**-collaboration [Tro+17]. It is a software for tracking of particles in electromagnetic fields. A user generated input file is used to define the geometry, which is then used by the electromagnetic field solver *KEMField*. The calculated fields and the geometry are then used to simulate the tracks of charged particles, by discretizing the flight path into steps and solving the equation of motion for each step. A more detailed view on *Kassiopeia* can be found in [Gro15] and [Beh16].

4.1.1 Geometry implementation

Implementing a geometry in *Kassiopeia* is done by the module KGeoBag. It offers geometrical classes for a lot of different shapes. Available shapes are divided into different types of surfaces and spaces. To construct a shape its necessary attributes have to be defined inside a **XML**-configuration file. Therein each shape is constructed in its own coordinate system, as seen in the following example.

```
<box_space name="box_A" xa="0.0" ya="0.0" za="0.0"
xb="1.0" yb="1.0" zb="1.0"/>
<cylinder_space name="cylinder_C" z1="-0.4" z2="0.4" r="0.3"/>
<disk_surface name="disk_a" z="0.0" r="0.1"/>
```

There is also the possibility to create arbitrary shapes by defining a set of points, that are either connected by lines or arcs. This poly-line then can be extruded or rotated to create non-trivial shapes.

In KGeoBag surfaces and spaces have to be related to each other to form a nested relationship. Spaces can contain other spaces and surfaces and these child shapes have to be completely contained inside the nesting parent.

Multiple transformations can be done on child shapes with respect to the coordinate system of its nesting parent. This includes transformation and rotation, as seen in the following example, using the shapes from the previous example.

```
<space name="outer_box" node="box_A">
<space name="inner_cylinder" node="cylinder_C">
<transformation rotation_euler="90 60 -90"/>
<transformation displacement="0.5 0.5 0.5"/>
</space>
<surface name="inner_disk_a" node="disk_a">
<transformation rotation_euler="90 45 -90"/>
<transformation displacement="0.5 0.5 0.8"/>
</surface>
</space>
```

A visualization of this example is shown in figure 4.1, next to its corresponding geometry tree.

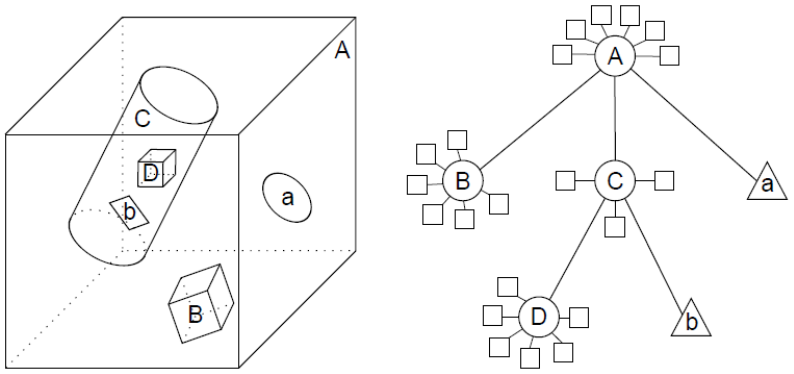

(a) Nested spaces and surfaces (b) Tree structure

Figure 4.1: A set of nested spaces and surfaces (a) and its represantation as a tree structure (b). In this example circles represent spaces, squares represent boundary surfaces and triangles represent free surfaces.

The geometrical shapes of the *KGeoBag* module feature an extension system which allows to append arbitrary information to the object. These extensions may contain different kinds of data for surfaces and spaces and can be used e.g. for visualization purposes, by appending colour to a shape or surface or assigning physical attributes, like the potential on a surface or the current through a space. As an example a current is allocated to the cylinder used in the previous example.

```
<electromagnet spaces="outer_box/inner_cylinder" current="50"/>
```

4.1.2 Particle Tracking

Integrating the equations of motion, which are given as first order ordinary differential equations. KASSIOPEIA offers several trajectory types, differing in the variables used to describe the physical state of the particle. Two of these types of trajectories used in the scope of this thesis are being presented here. Figure 4.2 explains the difference in trajectories used.

- **Exact Trajectory:** In the exact trajectory the equation of motion of a particle is described by the time t, its position $\vec{r}$ and its momentum $\vec{p}$, through the Lorentz equation,

$$\frac{d\vec{r}}{dt} = \frac{\vec{p}}{\gamma m}$$
$$\frac{d\vec{p}}{dt} = q\left(\vec{E} + \frac{\vec{p}\times\vec{B}}{\gamma m}\right),$$

  with the rest mass m and the relativistic Lorentz factor γ.

- **Adiabatic Trajectory:** If the adiabatic approximation (eq.3.1) is fulfilled, the particle can be described by its time t, the position of the guiding centre of the motion $\vec{r}_c$, the momentum components parallel and perpendicular to the magnetic field: $\vec{p}_\parallel$ and $\vec{p}_\perp$, as well as the gyration phase ϕ.

$$\frac{d\vec{r}_c}{dt} = \frac{p_\parallel}{\gamma m}\frac{\vec{B}_c}{B_c}$$
$$\frac{dp_\parallel}{dt} = -\frac{p_\perp^2}{2\gamma m B_c}\left(\vec{\nabla}B_c + q\vec{E}_c\right)\cdot\frac{\vec{B}_c}{B_c}$$
$$\frac{dp_\perp}{dt} = \frac{p_\parallel p_\perp}{2\gamma m B_c}\vec{\nabla}B_c\cdot\frac{\vec{B}_c}{B_c}.$$

  A smaller curvature in the propagation of the guiding centre position allows for a much larger step size, when using the adiabatic trajectory. The exact position of the electron is recreated from the guiding centre position afterwards.

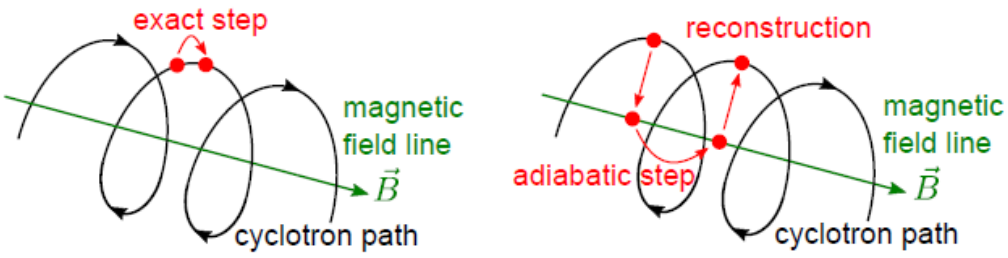

(a) Exact trajectory (b) Adiabatic trajectory

Figure 4.2: Scheme of the exact trajectory (a) and adiabatic trajectory (b) used in KASSIOPEIA. In the adiabatic trajectory the guiding centre is propagated and the exact position is recreated afterwards, allowing for a larger step size.

4.2 Katrino Electromagnetic Design

The electromagnetic design chosen for the tabletop spectrometer called Katrino in this thesis, is an improved version of an older setup analysed prior to this thesis.
To give a better explanation on the chosen setup, the old setup and the problems observed with that design will be reviewed shortly, before the simulation of the current spectrometer is explained.

4.2.1 Original setup and problems

The first setup was designed after the Mainz, Trotisk and KATRIN experiments and can be seen in figure 4.3. Two cylindrical magnets are located on a common symmetry axis. The source and detector are then placed on the sides of the magnets that are facing each other, so that the electrons travel on the magnetic field lines that span between the two magnets.
The distance between the two magnets is 250 mm. The magnets themselves are hollow cylindrical $N52$ Neodym magnets, with an inner diameter of 6 mm, an outer diameter of 40mm and a length of 40 mm. On top of both magnets a cap is put, as a holding structure for the detector and source, respectively. The cap itself reaches an additional 7 mm into the spectrometer with respect to the magnet. They produce an average field strength of ≈ 0.48 T at the position of the electron source. Towards the analysing plane the field strength drops down to $\approx 5 - 7.5$ mT. Magnet and cap are put on ground potential. In the introduction of the current setup in the laboratory in chapter 5.4 the cap will be investigated more closely.

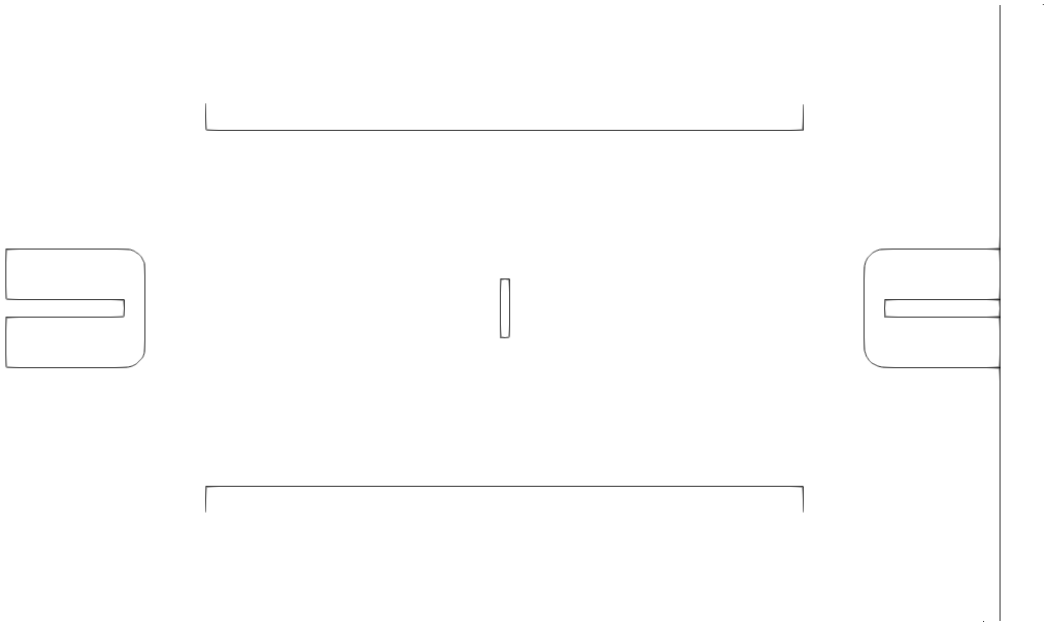

Figure 4.3: Cross section of the older setup designed after the KATRIN experiment, as it is implemented into the KASSIOPEIA software. The setup is implemented into a cylindrical chamber, with a length of 2 m and 300 mm diameter. The setup is mounted at one side of the chamber, which can be seen at the right side of the picture. The two hollow cylindrical $N52$ neodymium magnets, are 250 mm apart. Also shown is the cap that holds the magnets and the source or detector, respectively. In the center the 200 mm long and 120 mm diameter retardation electrode and the screening disk are shown.

A cylindrical shaped electrode is mounted in between the two magnets, to produce the analysing field of the spectrometer. It is 200 mm long and has a diameter of 120 mm. At both ends of the electrode an annulus extension is added to the electrode with a width of 10 mm and a rounded edge of 1 mm radius. The extensions are rounded to prevent field emission due to high electric fields.
Right at the centre of the cylindrical electrode, a disk with a diameter of 20 mm and a thickness of 1 mm is implemented. It is connected to the electrode via 3 holding poles, each with a diameter of 1 mm, giving the disk the same potential as the central electrode. The holding poles cannot be observed in figure 4.3, since the geometry implemented only contains axial symmetric components, to allow quicker computation times. Its primary use is to block soft x-ray radiation from the source, while it also acts to improve the homogeneity of the electric analysing potential.
The whole setup is placed inside a cylindrical vacuum chamber, with a length of 2 m and 300 mm diameter. The chamber is normally used as an UHV baking oven and was a temporary enclosure for the spectrometer.
With this geometry trajectories for 17.824 keV electrons from an isotropically emitting ^{83}Rb/^{83m}Kr source, implanted into a suitable substrate were tracked. An overview of the source parameters can be found in chapter 5.1. The tracking itself was done with the adiabatic approximation and a step size of 1/8 of a cyclotron motion.
Now the transmission function of the spectrometer was simulated, by starting Monte-Carlo runs for retardation voltages from -17.0 kV to -17.9 kV in 100 V steps. For each voltage 5000 tracks were started and then the number of electrons that pass the spectrometer and are detected should follow the MAC-E-Filter transmission function. The result of the simulations can be seen in figure 4.4.
The number of transmitted electrons follows the expected shape of a transmission function quite well in the slope region, but drops off towards higher surplus energies, as just above 50% transmission is reached. This behaviour points to a non-adiabatic guiding of the electrons.
From equation 3.1 it is expected that the adiabatic criteria is harder to fulfil the higher the surplus energy of the electron becomes, but another reason for the observed problems can be found when looking at the electric and magnetic fields inside the analysing plane.

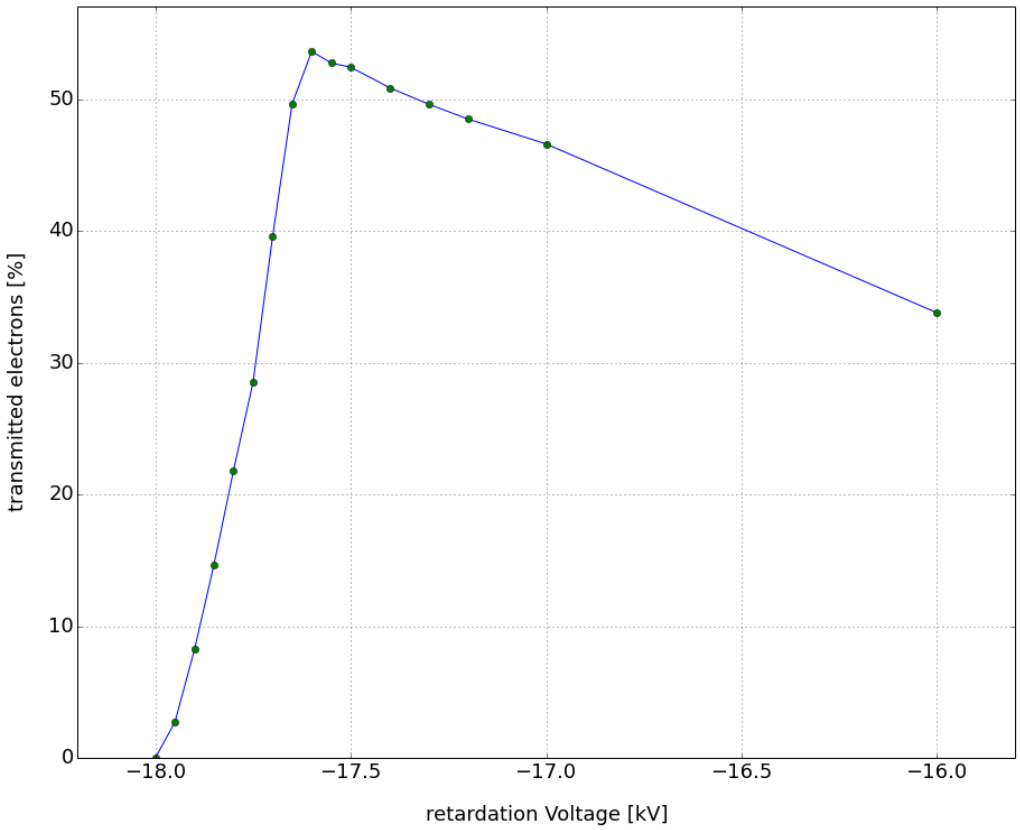

Figure 4.4: Simulation of the MAC-E-Filter transmission function. For each retardation voltage 5000 electrons with random source surface positions and an angular distribution expected from a isotropically emitting source were tracked.
The resulting transmission function follows the expected behaviour of a MAC-E-Filter transmission function for low surplus energies, but starts to drop off just above 50% transmission, due to field inhomogeneities.

Both fields show large inhomogeneities. The electric potential shown in figure 4.5 shows that the ground potential of the magnets has a strong reach through, while the inhomogeneity of the magnetic field, shown in figure 4.12, can be explained due to the non constant source field strength of the magnets. This inhomogeneity then also persists through the flux tube.
Both inhomogeneities lead to electrons with the same start position, but different starting angles experiencing different transmission conditions. The potential inhomogeneity also causes electrons to experience a force perpendicular to the magnetic field.

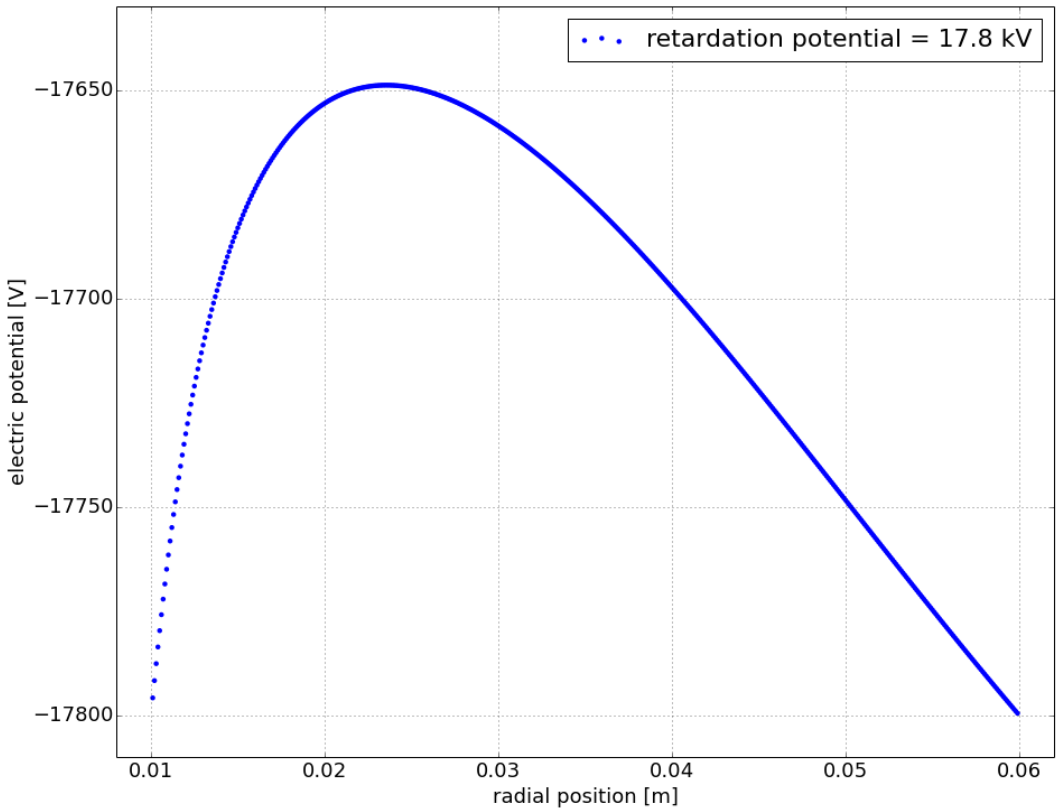

Figure 4.5: Electric potential in the analysing plane of the old Katrino setup. Visible is the large potential reach through that leads to electrons experiencing different transmission conditions depending on their phase.

This shows that this setup does not fulfil the conditions for a MAC-E-Filter properly. To investigate the reason behind the dropping transmission a look was taken at the termination condition of the electron trajectories. It showed that most electrons are magnetically reflected. Figure 4.6 shows the point of reflection inside the spectrometer and shows that the reflection occurs behind the analysing plane closely before reaching the detector.
This underlines the non adiabatic guidance of the electrons, that also leads to a non adiabatic energy transformation, thus leading to a magnetic reflection, since the magnetic field acts as a magnetic mirror behind the analysing plane, electrons that still have too much energy in their motion perpendicular to the magnetic field cannot reach the detector.

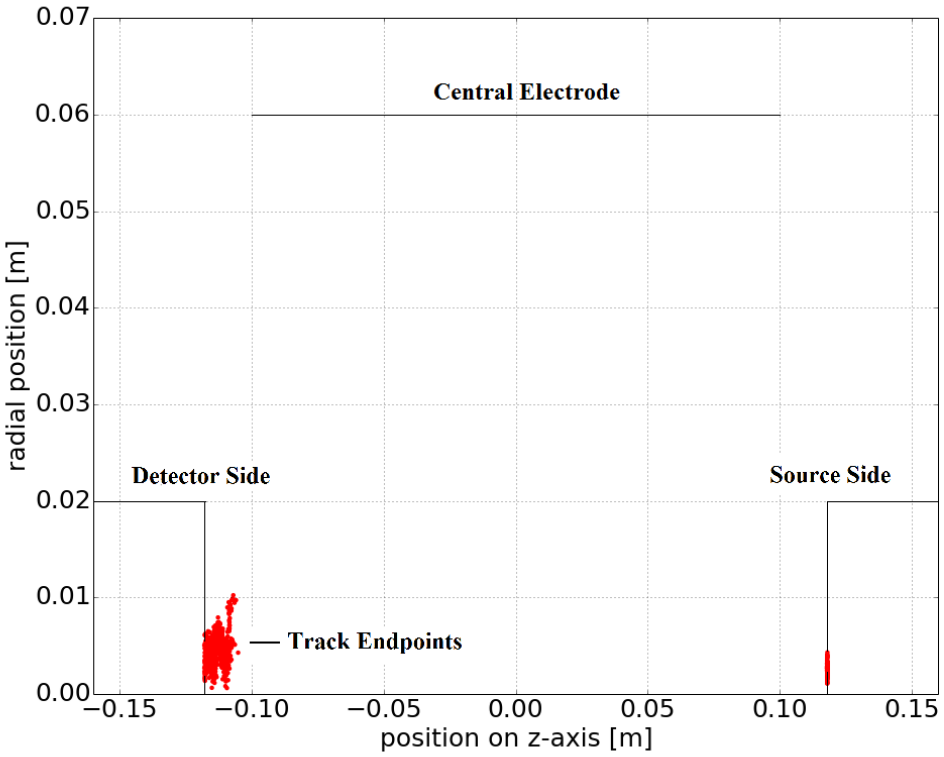

Figure 4.6: Points of termination (in red) of the simulated trajectories inside the old Katrino setup with a 17 kV retardation potential. A bunch of electrons is magnetically reflected just before reaching the detector on the left side of the picture, due to non adiabatic energy transformation.

4.2.2 The electrode system

In view of the problems with inhomogeneous fields, for the revised spectrometer introduced in the following, the focus was put on shaping the fields to be as homogeneous as possible. The new setup is an optimized version of the setup shown in the previous chapter. As long as not stated otherwise the components used are the same.
To tackle the problem of the inhomogeneous fields the new electrode was designed to enclose the flux tube as far as possible. Therefore conical shaped extensions have been added to the central electrode. They reduce the influence of the grounded magnets on the electric field in the analysing plane and help to make electric and magnetic fields parallel over a larger region of the spectrometer.
To fit these conical extensions into the existing setup the source and detector magnets have to be moved an additional 60 mm apart. Extending the distance between the ground potential and the analysing plane also decreases the reach through and lessens the inhomogeneity.
To determine the length and angle which the conical extensions should have in respect to the central cylindrical electrode, simulations for different parameters were performed. Figure 4.7 shows simulated transmission functions for different lengths of the extension, with a fixed angle of 55° with respect to the perpendicular of the central electrode.
It shows that the transmission already improves with respect to the transmission observed in the simulations for the old setup. For different lengths the transmission is very similar, until the length of the extension reaches 45 mm, where there is a clear loss of transmission at the upper slope.
This loss is due to the extension reaching to close to the magnetic flux tube and forcing the electrons to have higher energies to be transmitted. This is also known as too early retardation, since these electrons fulfil the transmission condition of the MAC-E-Filter, but are reflected on their way to the analysing plane where their transversal energy is still too large.
A feature in the simulated transmission functions is that the maximal transmission is reached at 80%. The missing electrons are lost due to collisions inside the spectrometer, which can be seen in all transmissions shown for the new setup. Electrons with starting angles $>\approx 80°$ collide with the caps at the source and detector, while a small portion also collides with the central disk.
Since a longer extension provides a better screening, we choose the longest suitable extension of 40 mm for further simulations on the angle in which the extension should be

implemented. The results of these simulations can be seen in figure 4.8, where the angle was varied from 10° to 60°.
For angles up to 40° the same phenomenon of too early retardation can be observed. For 10° the extension reaches so deeply into the magnetic flux tube that no electrons can pass through the filter. The transmission goes back to the expected shape at angles starting at 50°.

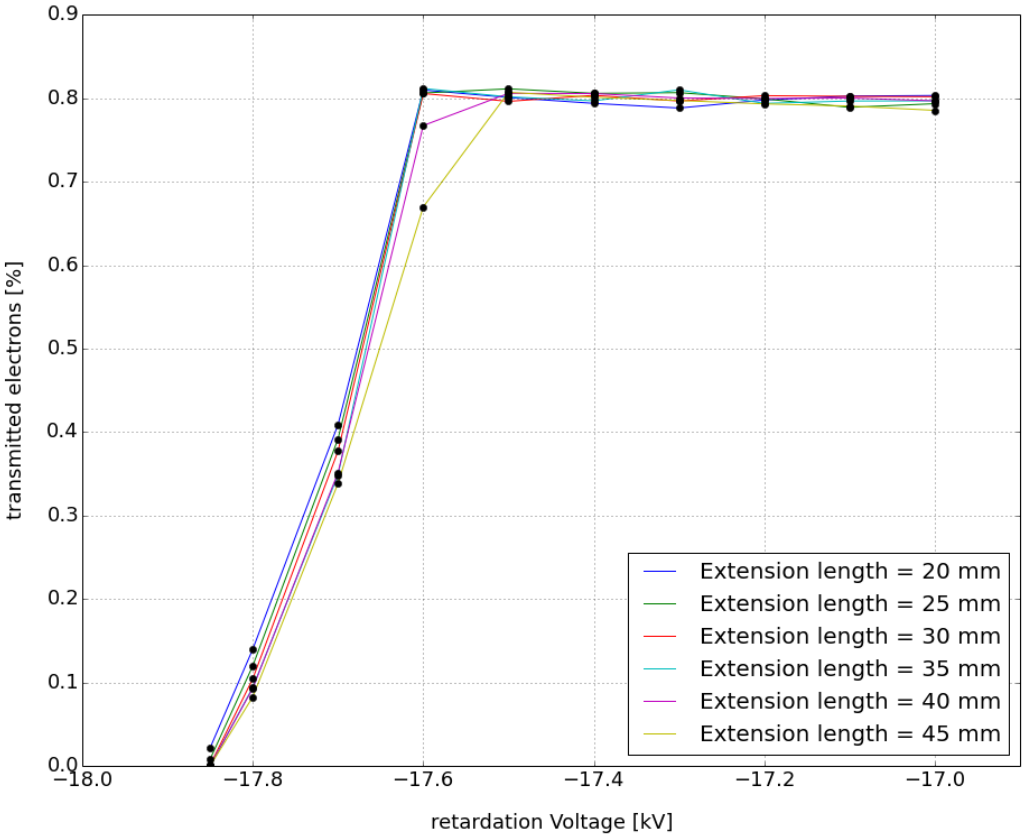

Figure 4.7: Transmission function of the Katrino spectrometer, for different lengths of the new conical shaped extensions of the central cylindrical electrode. For this simulation the extension has an angle of 55° with respect to the perpendicular of the cylindrical electrode.

The new design following from the simulations therefore has conical extensions that are symmetric to the analysing plane and are 40 mm long, with an opening angle of 60° with

respect to the cylindrical part. Source and detector magnet are 60 mm further apart than in the old setup. Figure 4.9 shows a cross section of the new design, with the magnetic field lines and the electric equipotential lines.

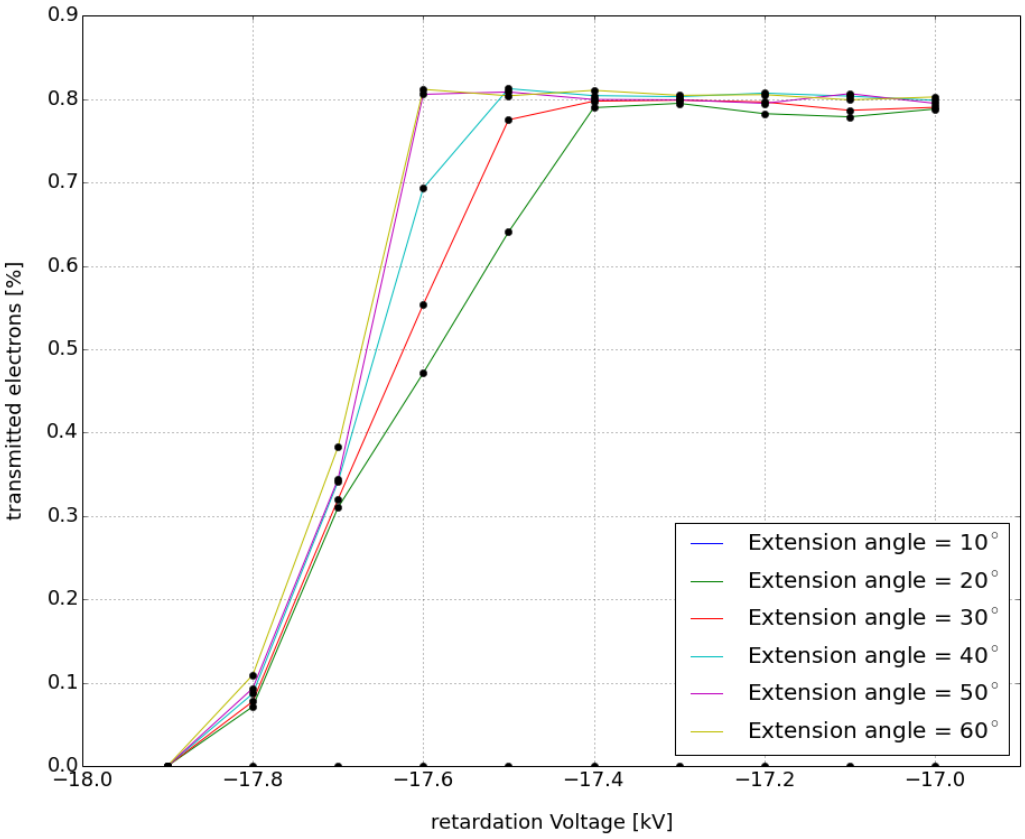

Figure 4.8: Transmission function of the Katrino spectrometer, for different angles of the new conical shaped extensions of the central cylindrical electrode. For this simulation the extension has a length of 40 mm.

The maximal electric field values reached inside the geometry occur between the central retardation electrode, with up to 20 kV and the magnets, lying on ground potential. To prevent problems with field emission, the maximum field strength should not exceed $\approx 10^6$ V/m. To keep the fields inside this limit, rounded edges with a radius of 8 mm were added to the conical extensions (see figure 4.10).

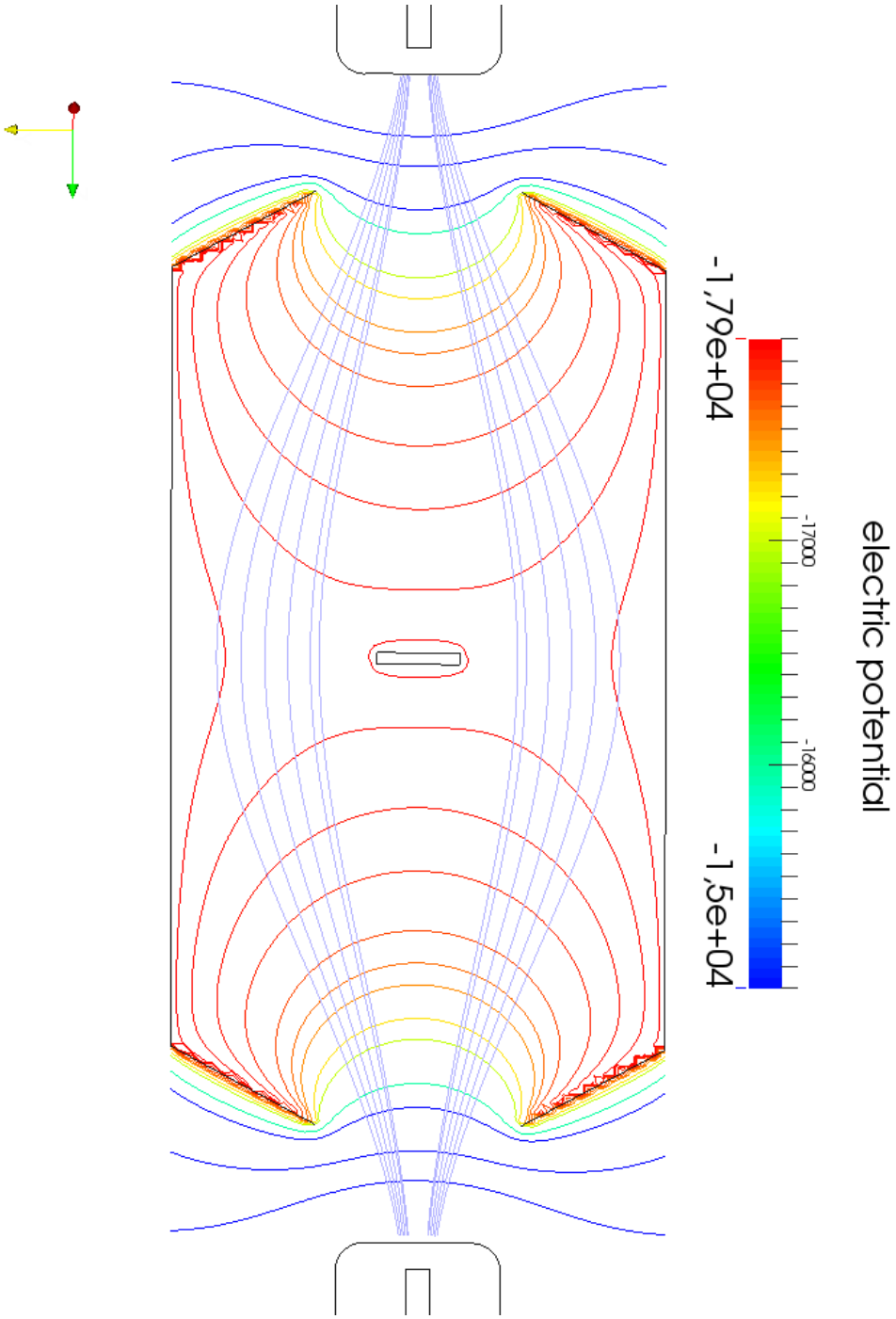

Figure 4.9: Cross section view of the current KATRINO setup, simulated in KASSIOPEIA and visualized with Paraview [AJG+05]. Visible are part of the magnets and the central electrode, with extensions and the screening disk. In rainbow colours the equipotential lines of the electric potential are shown. In grey the magnetic field lines are shown, that should ideally be oriented perpendicular to the equipotential lines in the whole spectrometer.

Figure 4.11 displays the inhomogeneity of the electric field in the analysing plane for the old and new setup. It can be seen that the changes introduced in this section reduce the potential differences from ≈ 150 V down to ≈ 5 V.
For the new setup a new cylindrical vacuum chamber, with a length of 600 mm and a diameter of 200 mm is used. In contrast to the old setup, this chamber was specifically modelled to fit the setup introduced. A more thorough description of all components can be found in chapter 5.2.

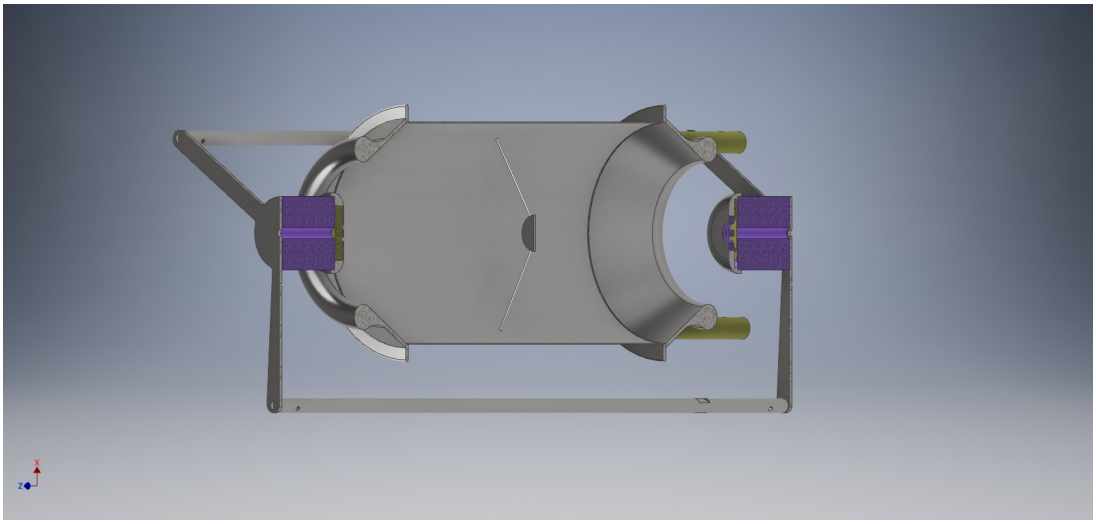

Figure 4.10: Cross section of the CAD model of the tabletop MAC-E-Filter spectrometer. In purple the magnets, producing the guiding field, are visible inside their holding structure, which is mounted directly to the top flange of the vacuum chamber. In the centre one can see the cylindrical spectrometer with conical extensions and a screening disk in its center to block x-ray radiation from the source. In olive the peek holding of the central electrode is visible, which is also mounted to the flange.

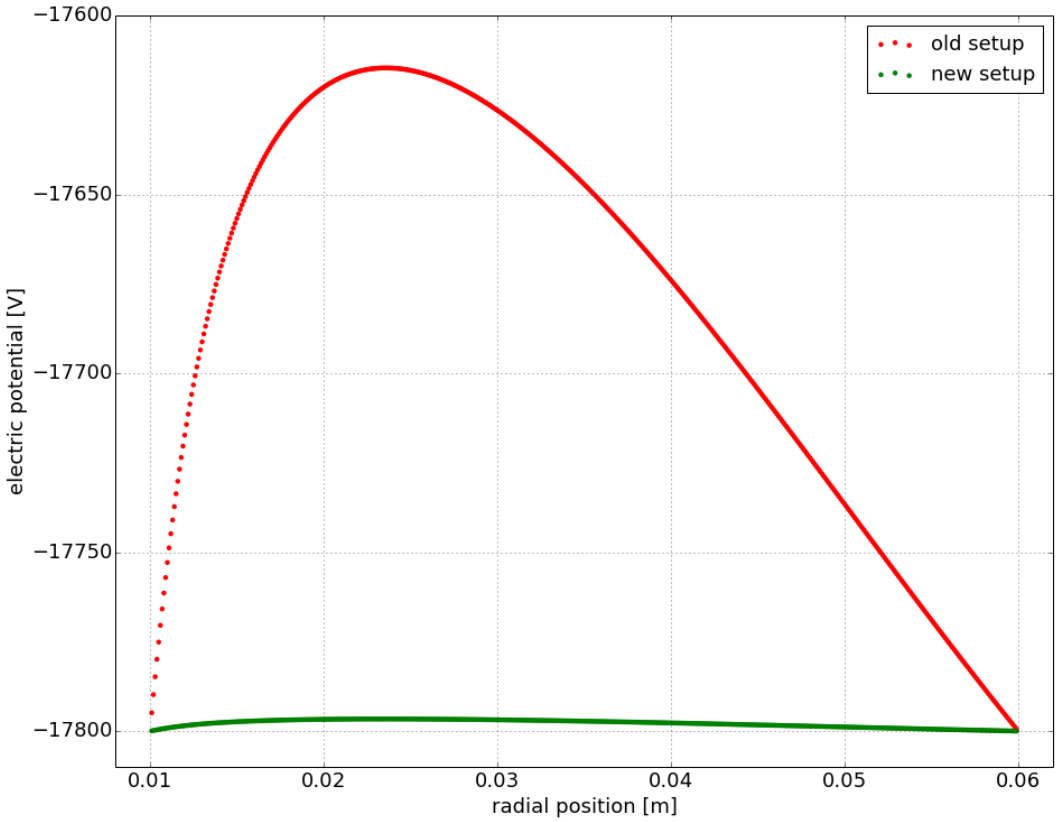

Figure 4.11: Comparison of the electric potential in the analysing plane, for the different setups introduced in this thesis. In blue the first version of the setup, with ≈ 150 V potential inhomogeneity is shown. The new setup is displayed in green with additional 30 mm distance on each side between ground potential and analysing plane and additional screening electrodes, reducing the potential inhomogeneity to ≈ 5 V.

4.2.3 Shaping of the magnetic field

Since the magnetic field naturally decreases in strength with increasing distance to the magnets the analysing field strength in the new setup drops to ≈ 4 mT, due to the increase in distance between the magnets. This also decreases the field inhomogeneity of the magnetic field in the analysing plane and improves the energy resolution. For an additional improvement of the magnetic field inhomogeneity in the analysing plane, an air coil is added to the setup to shape and strengthen the magnetic field.

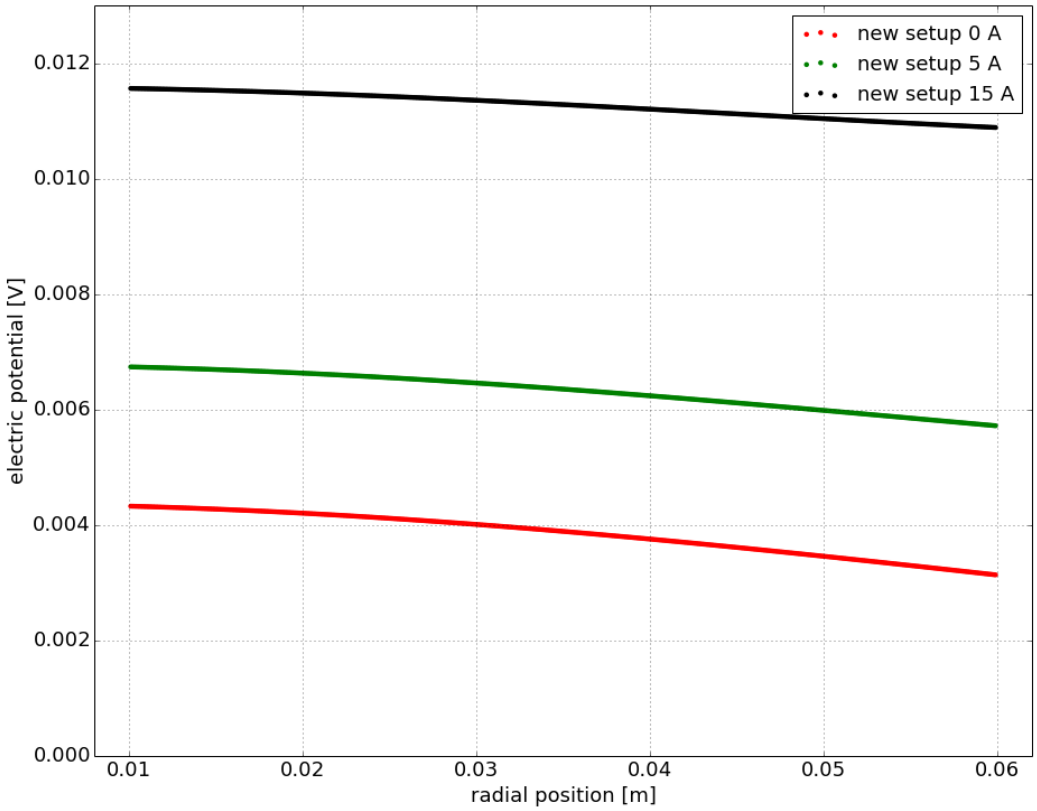

Figure 4.12: Magnetic field strength in the analysing plane of the Katrino setup, showing the effect of the air coil. A decreased field inhomogeneity can be observed for increasing coil current.

Luckily an air coil with the required field strength was still available [Hil11]. This air coil has a length of 100 mm, a inner diameter of 314 mm and a outer diameter of 450 mm.

The coil winding is explained in chapter 5.3. Simulations could show that it shapes the field in the desired way, as shown in figure 4.12.
Through the strengthening of the magnetic field the energy resolution is slightly reduced. Therefore, a trade off has to be made between field homogeneity and energy resolution. In figure 4.13 the simulated transmission of the spectrometer for air coil currents ranging from 1 A to 5 A is shown. The worsening energy resolution for higher fields is visible in the fact that the slope of the transmission slightly widens for higher magnetic fields. Also visible is that electrons with higher surplus energies are guided better through the spectrometer under a higher magnetic field and show constant transmission above 17.5 kV, as expected.

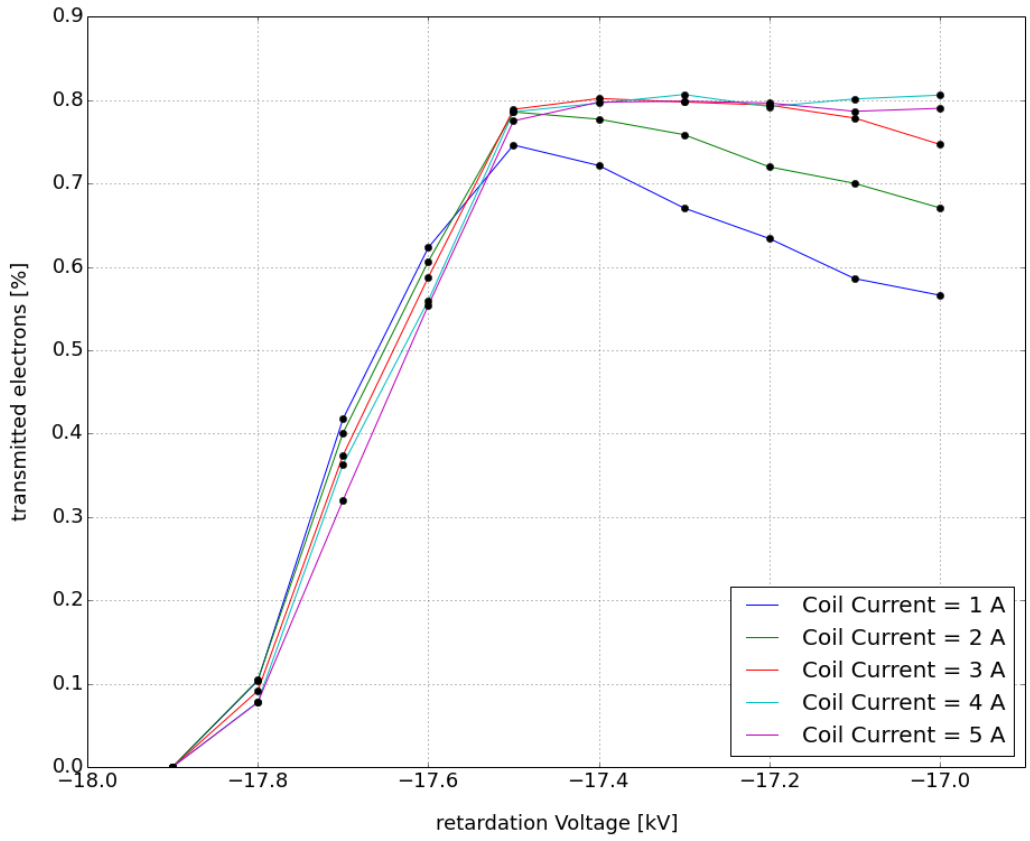

Figure 4.13: Transmission function of the tabletop spectrometer for air coil currents ranging from 1 A to 5 A. The simulated points in the slope region widen for higher magnetic fields, showing the expected decreasing energy resolution.

Figure 4.14 shows the transmission up to the maximal air coil current of 25 A. As the 5 A already shows the highest transmission, a higher air coil current would not benefit the spectrometer and only worsen the energy resolution.

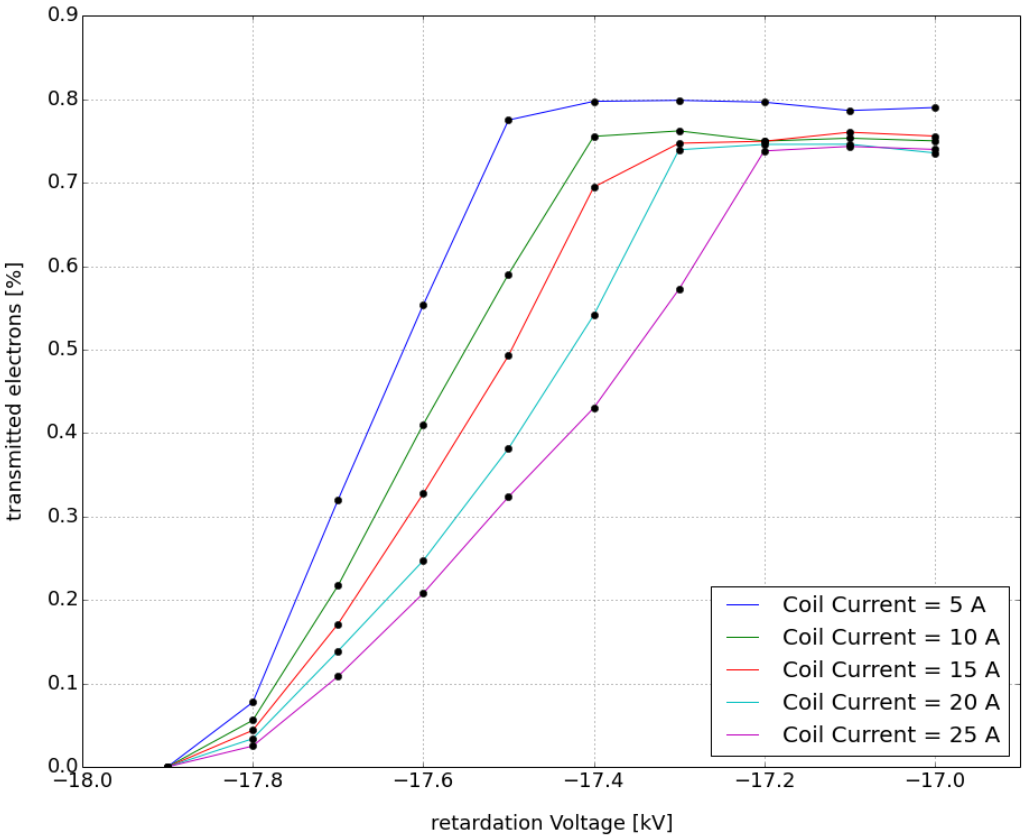

Figure 4.14: Transmission function of the tabletop spectrometer for air coil currents ranging from 5 A to 25 A. The transmission below 17.5 kV retardation voltage shows how the adiabatic guiding of the electrons improves for higher air coil currents. The simulated points in the slope region widen for higher magnetic fields, showing the expected decreasing energy resolution.

5 Assembly

On the basis of the previously discussed simulations, a tabletop spectrometer was constructed, built and tested in the laboratory in Münster. This chapter will introduce the components used in the setup.

5.1 ^{83}Rb/^{83m}Kr Source and Detector

The spectrometer was designed with the intent to measure the Tritium β-decay spectrum. But due to the easier availability, handling and with its 17.824 keV conversion electrons, relatively close to the tritium endpoint spectrum, ^{83m}Kr was chosen as a suitable replacement for tritium, for testing the spectrometer.

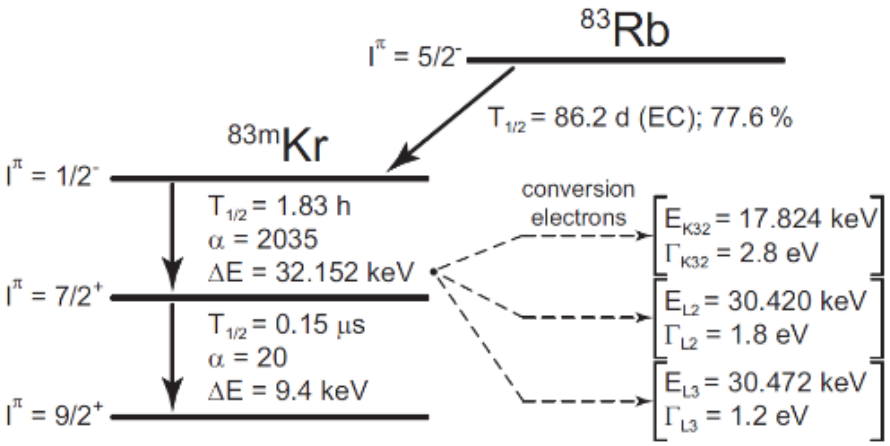

Figure 5.1: Decay scheme of ^{83m}Kr, which is produced via an electron capture decay of the mother isotope ^{83}Rb. It decays in a 2-fold process, producing multiple conversion electron lines. The energies of the relevant lines are shown in the picture.

With a half-life time of 86.2 d ^{83}Rb, the mother isotope of ^{83m}Kr, has a much higher life time as ^{83m}Kr with 1.83 h. The mother isotope ^{83}Rb decays into the isomeric state ^{83m}Kr with a probability of 77.6 % via electron capture. Multiple electron lines are produced, when ^{83m}Kr de-excites through the process of internal conversion. The isomeric state has an excitation energy of 41.55 keV and decays via an intermediate level with an energy of 9.4 keV, see figure 5.1. Thus the energy of the first transition is 32.151 keV, with a conversion coefficient of $\approx$ 2000. The conversion electrons stemming from the K-shell

have a kinetic energy of 17.824 keV, with a line width of 2.71 eV. Conversion electrons with energies of ≈ 30.4 keV are produced from the atomic L-shells while M-shell electrons are observed at ≈ 32 keV. Conversion electrons from the 9.4 keV γ transition have to low energies to be resolved from the noise of our detection system.
The sources came in the form of ^{83}Rb implanted into either platinum or **H**ighly **O**riented **P**yrolitic **G**raphite (HOPG). Figure 5.2 shows a radiographical image of the activity distribution on the platinum substrate taken in the PhD thesis of Martin Slezak [Sle15]. The active area has a diameter of ≈ 2.75 mm $- 5.5$ mm.
As a detector a windowless Si-PIN photodiode (Hamamatsu S3590 $-$ 09), with an active area of 10×10 mm is used. The data sheet can be found in the appendix 8.3.

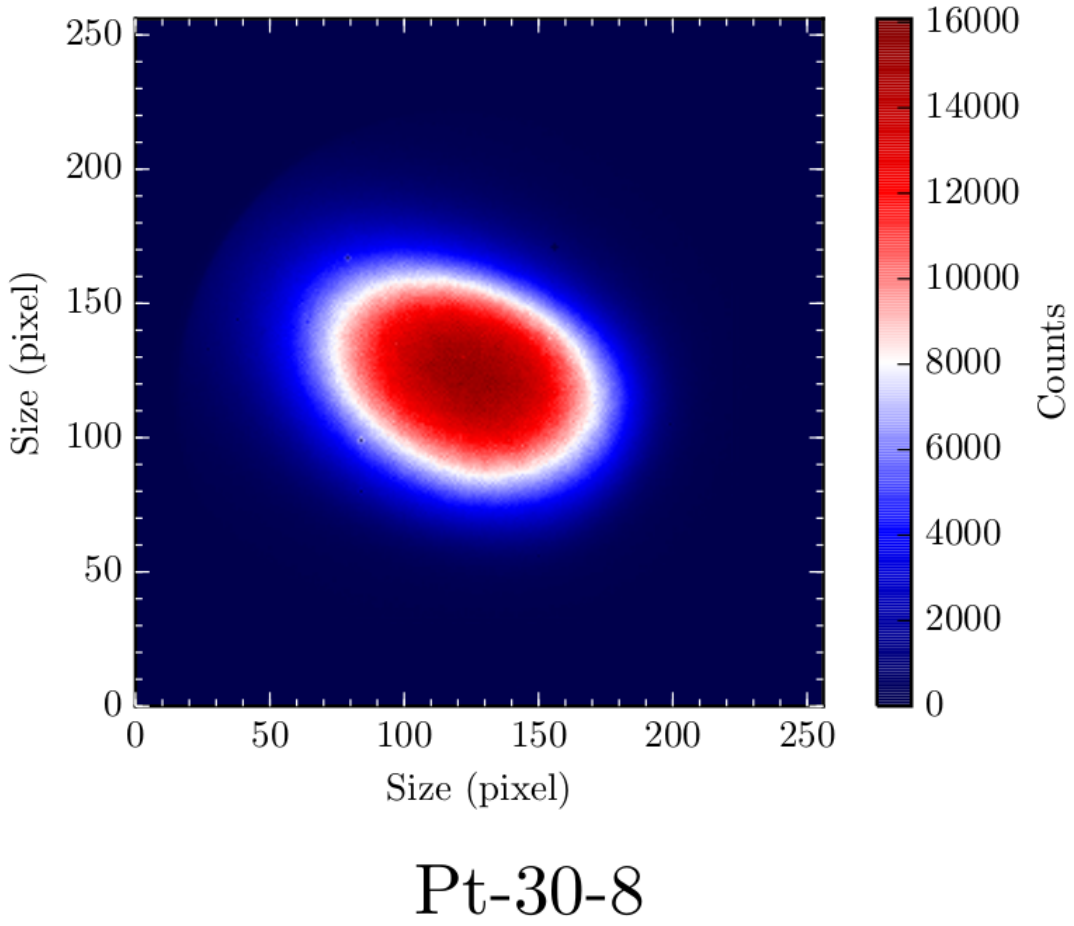

Figure 5.2: Radiographical image of the source used inside the old Katrino setup. The image was taken with a timepix detector of 256×256 pixels [Sle15]. The active area has a diameter of ≈ 2.75 mm $- 5.5$ mm.

5.2 Vacuum and Electronic system

In this section the current setup in the laboratory in Münster is introduced. The spectrometer is located inside a cylindrical 600 mm long and 200 mm diameter vacuum chamber, with CF200 flanges at each end. Figure 5.3 shows the assembled chamber in the laboratory.

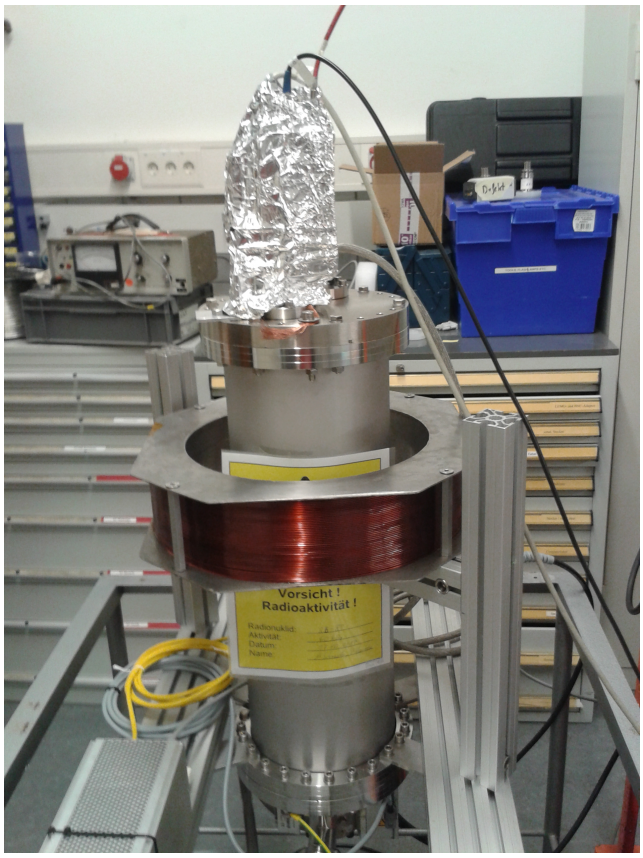

Figure 5.3: Laboratory Setup in Münster. Visible is 1) the vacuum chamber 2) the preamplifier mounted at the top, on the detector output, which is wrapped in aluminium foil to lessen the noise, 3) the air coil to shape the analysing magnetic field.

As retardation voltages up to 20 keV are used inside the setup, pressures below 1×10^{-6} mbar are necessary. For the vacuum operation two adapter flanges on the bottom CF200 flange are used. A CF63 flange connects to the Pfeiffer TMU 071 P turbo molecular pump, which creates vacuum conditions of $\approx 1{\cdot}10^{-7}$ mbar in the before mentioned vacuum chamber. To create the desired prevacuum a Pfeiffer MVP $070-3$ pump is connected to the outlet of the turbo molecular pump. The second CF40 adapter flange connects a pressure gauge (Leybold ITR 200) to the chamber.

The spectrometer is mounted on the top flange such that the magnet with the detector on top is directly sitting on the top flange. In this way the connection from the detector to the preamplifier is as short as possible, to lessen the noise. The top flange contains two connections. One for the high voltage feed through and one, where the preamplifier is connected to the detector. The preamplifier was built in the electronics workshop of the institute after a design used in the Mainz neutrino mass experiment. It is a charge sensitive preamplifier with very low noise amplification [Sch90].
The modules for the voltage supply of the detector and the readout process are mounted into a NIM crate, which can be seen in figure 5.4. A NHQ 224M module is used as a bias voltage supply for the detector. For determination of the dead time of the acquisition system a ORTEC model 419 pulser is operated at 50 Hz. Signal processing is done by a Model 7614 Amplifier, from Silena Milano. The amplifier signal is processed by a FASTComTec MCA-3 ADC.

Figure 5.4: Picture of the components for readout and detector voltage supply mounted into a NIM Crate, from left to right, the Silena Milano Amplifier Model 7614, ORTEC model 419 50 Hz pulser and the high voltage supply NHQ 224M module.

The voltage supply of the electrode system is a Knürr-Heinzinger PNC 5 30000 − 5 neg, providing up to −30 kV, mounted into a 19" rack, which also contains the power supply of the air coil, described in the next subchapter.

5.3 Aircoil

The air coil used in the setup was built for the dissertation work of Björn Hillen [Hil11]. In this work, for shaping of the magnetic field only small field strengths are needed, so no cooling of the coil is required.
The coil allows currents up to 25 A in permanent mode, which corresponds to a field strength of 12 mT in the center of the coil.
The coil is made of copper lacquered wire, with a diameter of 2.1 mm and a lacquer thickness of ≈ 0.05 mm. It is made of 8 parallel connected coils, with a length of ≈ 140 m wire each, to reduce the overall resistance of the coil. The single coils are connected via epoxy glue, for mechanical stability.

5.4 The electrode system

The main features of the setup have already been discussed in chapter 4.2.2, so only components that were not discussed there, or implemented differently then mentioned will be discussed here.
The central retardation electrode is held by 2 poles that are mounted on the top flange. They are 99 mm long and have a diameter of 12 mm. Due to the fact that this setup is an upgraded version of an older setup, the poles are made of a 69 mm long part that is made of PEEK isolator and a part made of stainless steel, which was added due to the lengthening of the setup.
A picture of the electrode structure can be seen in figure 5.9.
The support for the magnets is a cap with a spherical cross section that has a diameter of 44 mm at its widest part. At the top it has a spherical surface with a diameter of 30 mm that is parallel to the magnets spherical end surface. The total length amounts to 10 mm, of which 7 mm lay above the magnet (figure 5.6).
The caps provide a cylindrical cavity, which is used to house the source and detector on the two magnets, respectively. Both cavities have a depth of 6.5 mm. Source and detector are placed inside PEEK holdings that fit into the cavity beneath the cap and can be seen in figure 5.6 and 5.7 respectively.
Both caps offer an annulus opening for the electrons to pass through. This implements

another disk in front of the source and detector respectively for further screening of soft x-rays stemming from the source. The annulus opening has an 11 mm outer diameter and 3.8 mm inner diameter for the detector cap and 9 mm outer diameter and 4.6 mm inner diameter for the source, see figure 5.5 and 5.8 for the source magnet and detector magnet holding respectively. The opening of the detector is wider for a larger detection area. The positioning of the annulus surface was chosen such that the magnetic field lines that guide the electrons are curved enough inside the spectrometer such that collision with the central disk is prevented as far as possible.

Figure 5.5: Close up of the magnet cap of the source, showing the annulus opening inside the cap, allowing for the electrons to pass through. The source material as well as the holding material are visible and show the off axis implementation of the source.

The cap is mounted via 3 legs to the underlying holding structure. This is a spherical plate with the same radius as the magnet. From this plate 3 legs with a width of 10 mm and a length of 78 mm connect to a 390 mm long and 8 mm wide pole each. These poles connect the holding structures of the two magnets such that one magnet is hanging in the vacuum, see figure 5.9.

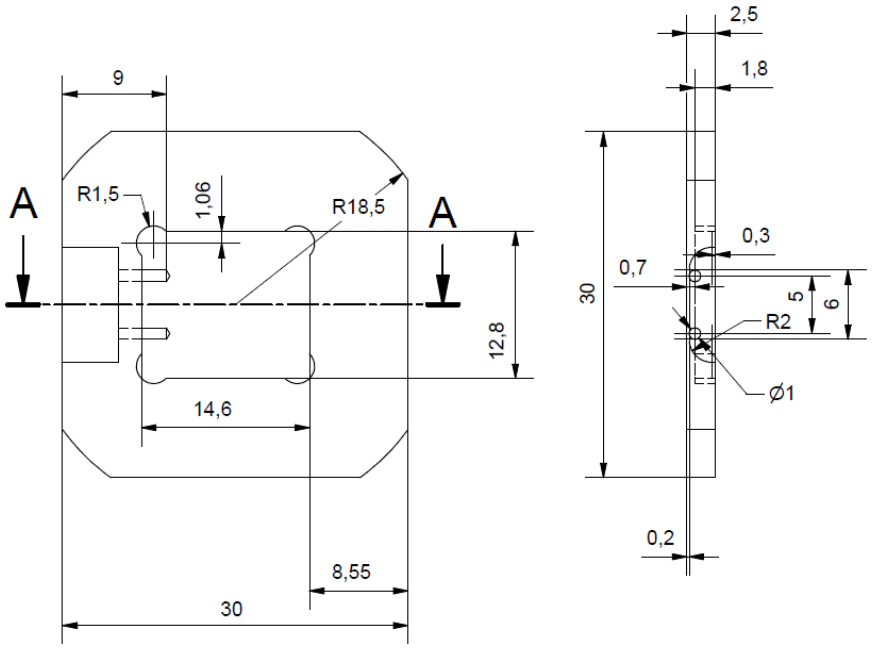

Figure 5.6: Technical drawing of the PEEK Holding of the detector, which is hold on top of the magnet with the holding structure shown in figure 5.8.

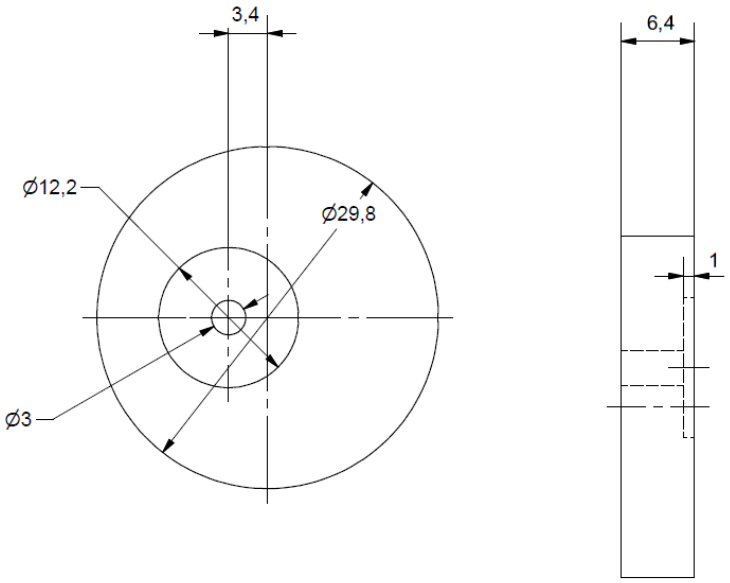

Figure 5.7: Technical drawing of the PEEK Holding of the source, which is hold on top of the magnet with the holding structure shown in figure 5.5.

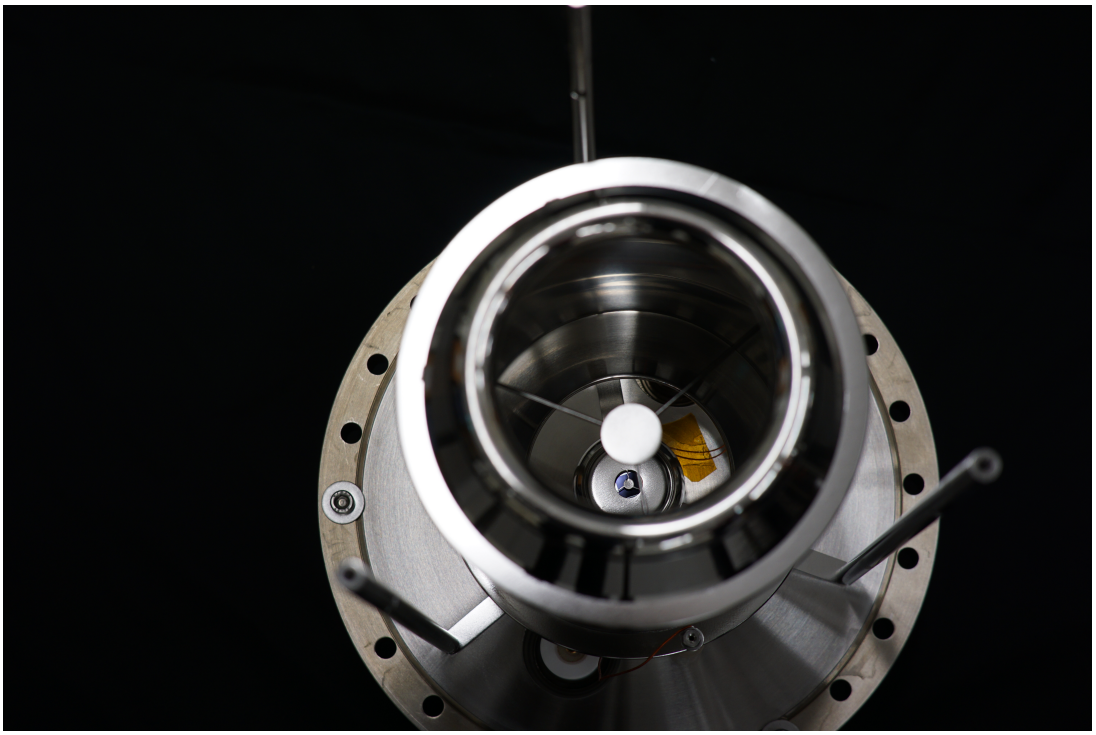

Figure 5.8: View of the inside of the spectrometer. The source holding has been unmounted, so that this picture of the inside was possible. The detector inside his holding structure is visible at the other end of the spectrometer.

Figure 5.9: Picture of the electrode structure implemented in the laboratory in Münster. Visible are the central electrode, the poles that connect the magnet holdings and the magnets under the caps that fixate them.

6 Measurement and Analysis

6.1 Data sets

In first measurements the goal was to see if the expected retardation of the 17.8 keV line could be observed, when varying the applied voltage over the electron energy and whether or not the measured rates would follow the transmission function expected from a MAC-E-Filter.
For this purpose a fix coil current of 15 A was applied, which corresponds to a strengthening of the magnetic field in the center of the analysing plane to 11 mT. Then the Voltage was varied from −16.0 kV to −19.0 kV in 100 V steps. For each step 300 s of data were taken. An overlay off all measured spectra can be seen in figure 6.1, which shows the total count rate against the channel number of the ADC. In different colors from blue to red, the different measurements are shown in order, starting from −16.0 kV voltage, to −19.0 kV. To determine the dead time of the detector, a pulser with a frequency of 50 Hz was applied to the preamps test input. The corresponding pulser peak is at higher channel numbers outside the range shown in figure 6.1.

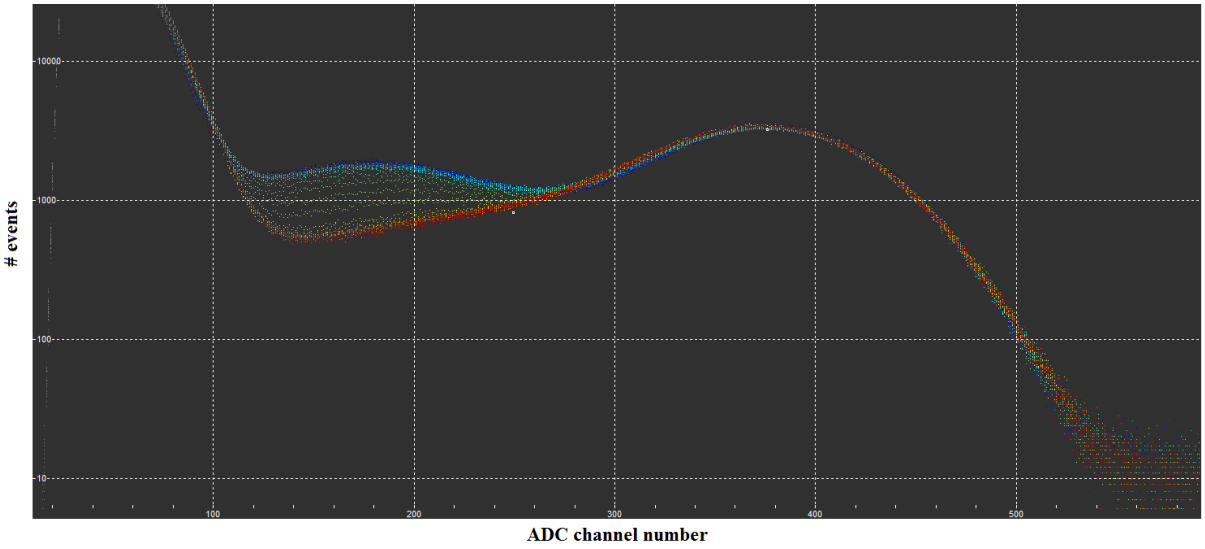

Figure 6.1: All 31 Spectra of the 15 A measurement, for −16.0 kV to −19.0 kV retardation voltage. The spectra are colored from blue to red starting from the −16.0 kV spectrum.

As expected, a decrease of the 17.8 keV peak can be observed, while the mixed peak of 30 keV and 32 keV electrons at higher channel numbers does not change over the ob-

served range of voltages. The residual count rate observed at retardation voltages above 17.8 keV is caused by background electrons stemming from the central electrode system. These background electrons are produced by soft x-rays from the ^{83}Rb/^{83m}Kr source hitting the electrode material and are subsequently accelerated by the negative potential of the electrode. They therefore occur at an energy corresponding to the retarding voltage in the spectrum.
In a second measurement a coil current of 5 A was applied (see figure 6.2), corresponding to 6.3 mT magnetic field strength in the analysing plane. This time the voltage was varied over −16.7 kV to −18.3 kV, in expectance of a sharper transmission function. To get a better resolution of the slope of the transmission function, the voltage was varied in 50 V steps, in the interval −17.3 kV to −17.9 kV. For the other voltages again a step size of 100 V was chosen and the measurement time is again 300 s per voltage step.

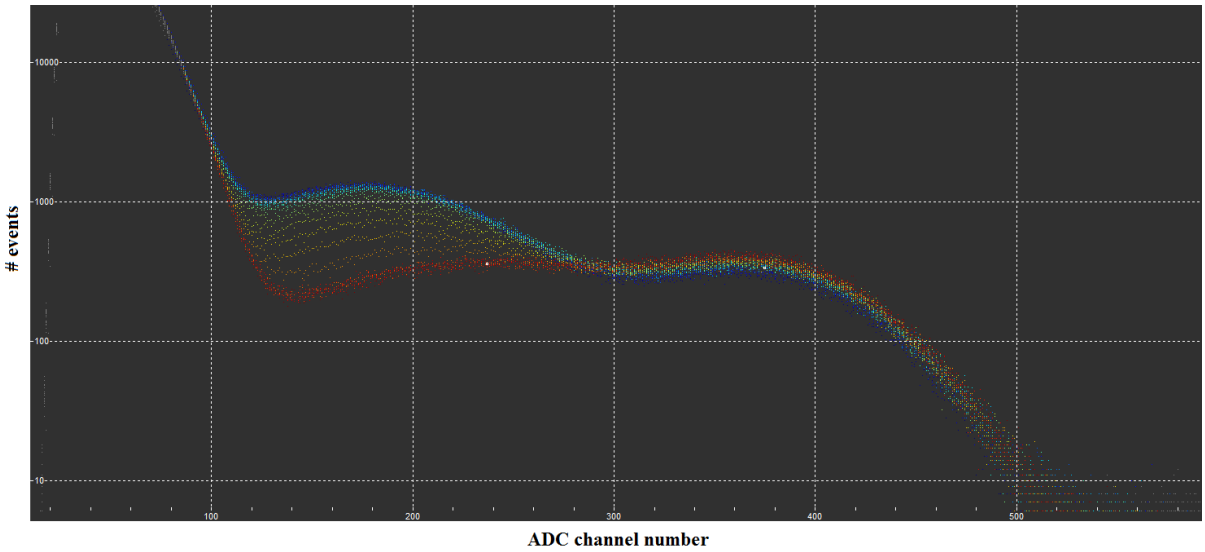

Figure 6.2: All 23 Spectra of the 5 A measurement, for −16.7 kV to −18.3 kV retardation voltage. The spectra are colored from blue to red starting from the −16.7 kV spectrum.

We can observe the same two peaks in this measurement, with the same qualitative change.
Interesting is that the height of the mixed 30 keV peak is about a magnitude lower in the 5 A measurement. Since these electrons do have quite large surplus energy, they have quite large cyclotron radii in the analysing plane and collide with higher probability with the central electrode at the lower magnetic field settings. As such the higher magnetic field provides a better guiding for these electrons.

6.2 Fits and Analysis

As an example for the analysis of a single measurement the fit to the 17.8 kV data, with a coil current of 15 A, is shown in figure 6.3. All fits have been made with the fitting program fityk [Woj]. With a variety of predefined functions and the ability to add functions via its graphic interface, it allows quick data analysis.

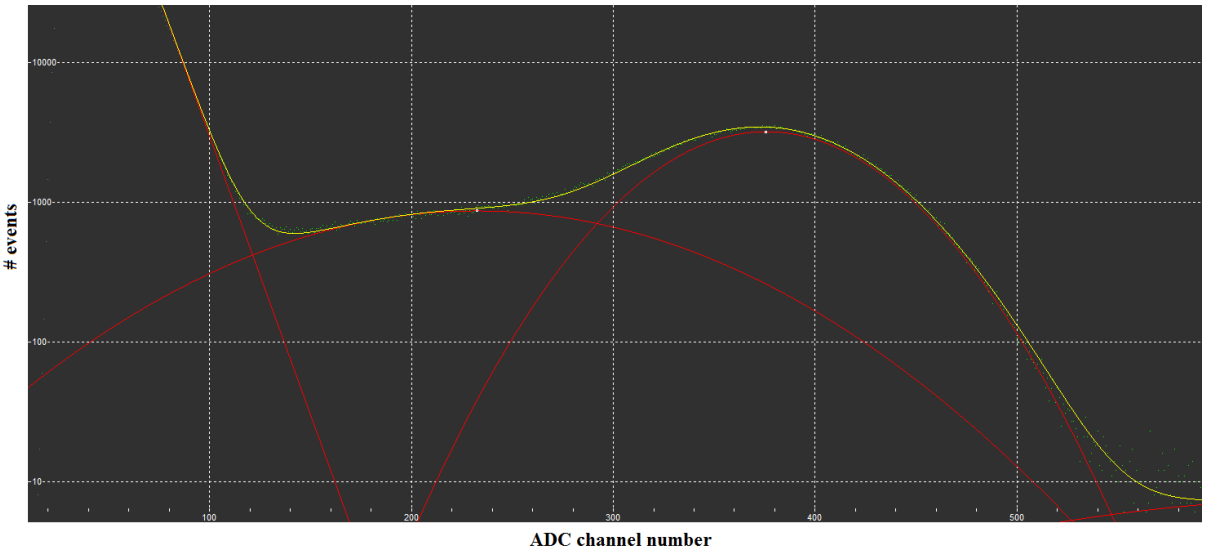

Figure 6.3: Spectrum of the 17.8 kV measurement, at 15 A coil current, shown in a logarithmic scale. In red the separate fit functions, in yellow the sum of the fit functions is shown and behind the fit in green the data points.

Both peaks observed in the spectrum can be fitted via a gaussian function. While the line shape of the source is lorentzian, its width is only in the order of a few eV. Thus the energy resolution of the detector dominates the peak shape.
The low energy electronic noise is fitted via an exponential curve. To investigate if the decrease of the 17.8 keV peak with increasing voltage is in agreement with the MAC-E-Filter transmission function, the area of the corresponding gaussian was plotted against the retardation voltage and then fitted with the analytical transmission function of the MAC-E-Filter, letting the amplitude, the background and the ratio of the minimal and maximal magnetic field be fit parameters. These fits are shown for the 15 A measurement and the 5 A measurement in figure 6.4 and 6.5, respectively.
As can be seen the fit describes the data qualitatively, but especially the upper edge of the slope is not described well through this method.

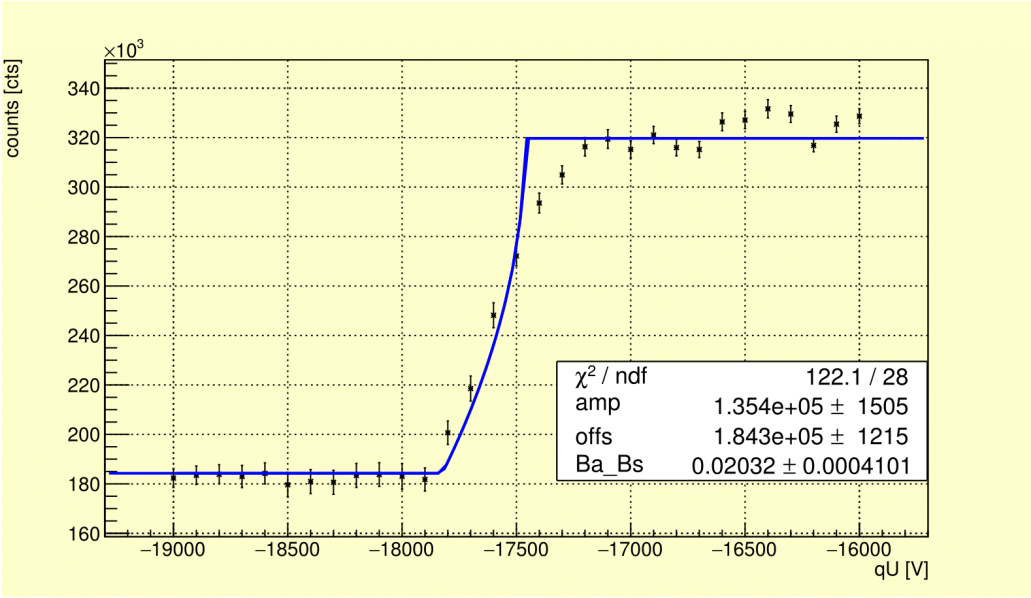

Figure 6.4: Transmission function fit (blue) for the 15 A coil current measurement, using the analytical transmission function of the MAC-E-Filter, shown in equation 3.6. Free fit parameter are the ratio of the minimal and magnetic field, as well as the amplitude and background rate. The data points correspond to the area under the Gaussian fit of the 17.8 keV peak.

Still the fitted ratio of the magnetic fields corresponds reasonably well with the expected results of $B_{ana}/B_{src}(15\text{ A}) = 6.3\text{ mT}/0.48\text{ T} \approx 0.013$ and $B_{ana}/B_{src}(5\text{ A}) = 11\text{ mT}/0.48\text{ T} \approx 0.023$.

A more careful analysis of the measured transmission functions needs to take energy losses in the source into account, which occur when electrons experience multiple scattering while travelling through the HOPG material. These energy losses depend on the implantation energy of ^{83}Rb into the material (which determines the depth in which the atoms are implanted) and are reported in the PhD thesis of M.Slezak [Sle15] for ^{83}Rb implanted into Platinum, for different implantation energies.
To include the energy losses into the fit, the calculated response function given by M.Slezak was convoluted with the transmission function used in the previous fit. The resulting fits can be seen in figure 6.6 and 6.7.
Comparing to the previous fits an improvement can be seen, but the upper slope region still is not fully represented.

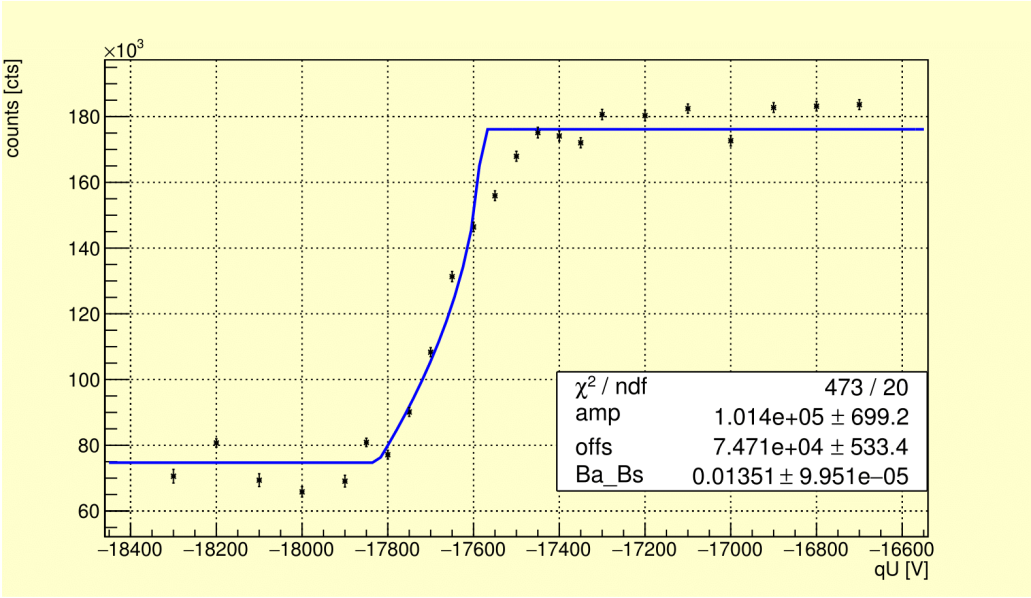

Figure 6.5: Transmission function fit (blue) for the 5 A coil current measurement, using the analytical transmission function of the MAC-E-Filter, shown in equation 3.6. Free fit parameter are the ratio of the minimal and magnetic field, as well as the amplitude and background rate. The data points correspond to the area under the Gaussian fit of the 17.8 keV peak.

Another effect that seems to be present is caused by the phase dependence of the cyclotron motion on the retardation voltage, presented and simulated in the PhD thesis of Michael Zacher [Zac14]. Due to the limited detector size, a shift in phase can cause the electrons to miss the detector area. This effect leads to an oscillation in the number of electrons detected in the spectrometer. Such an oscillation is well visible in the 15 A data in the region of full transmission and to a lesser extend in the 5 A data as well. To quantitatively understand the effect of the phase shift and integrate it into the fit additional simulations would be required, which were not possible any more in the scope of this thesis.

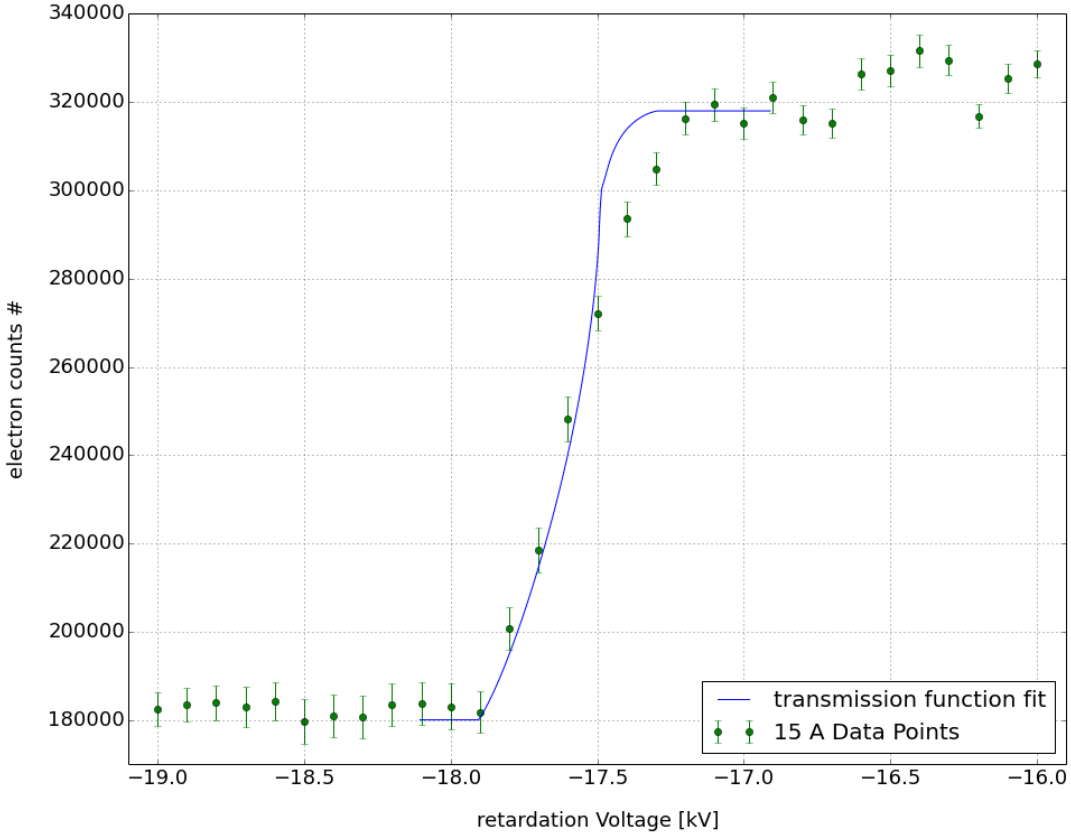

Figure 6.6: Transmission function fit (blue) for the 15 A coil current measurement, using a convolution of the analytical transmission function of the MAC-E-Filter and the energy loss function simulated by M.Slezak [Sle15].

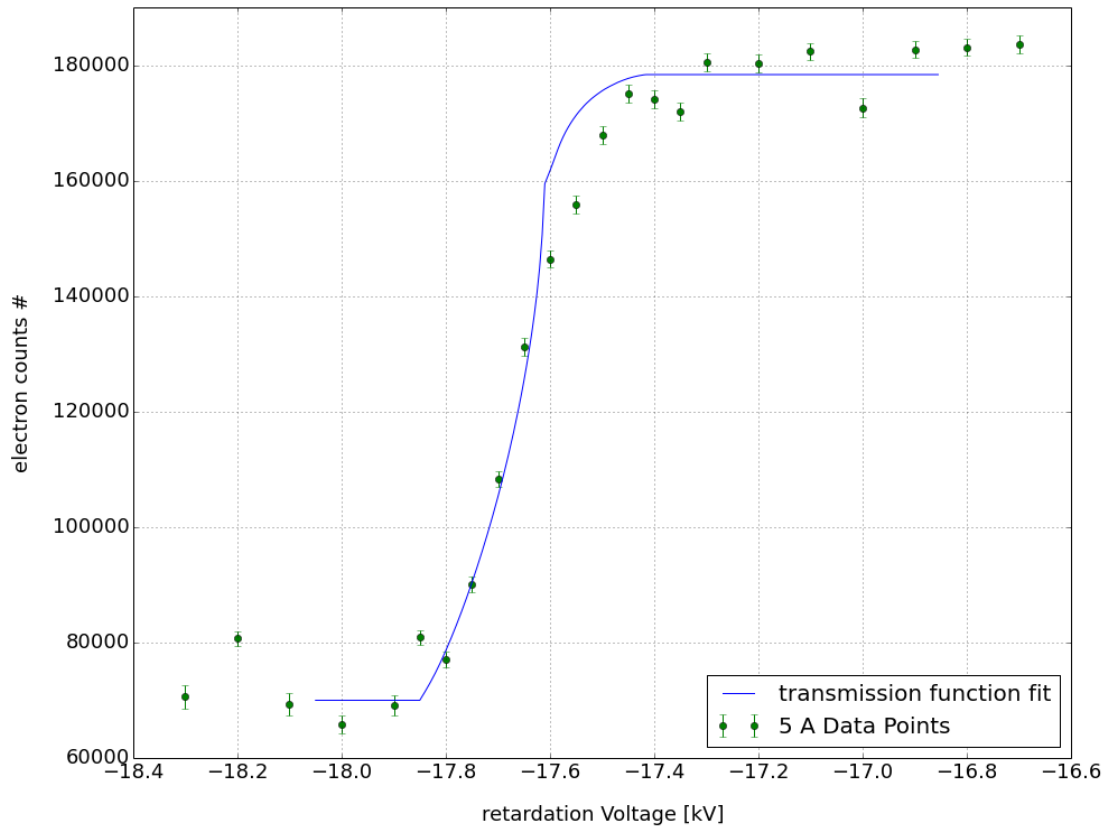

Figure 6.7: Transmission function fit (blue) for the 5 A coil current measurement, using a convolution of the analytical transmission function of the MAC-E-Filter and the energy loss function simulated by M.Slezak [Sle15].

7 Summary and Outlook

The MAC-E-Filter principle has been used in several past and ongoing experiments measuring high precision tritium β-spectra to determine the neutrino mass [Kra$^+$13, Ase$^+$11]. The spectrometers used in these experiments are at least a few meters in length. Building and commissioning a tabletop spectrometer using the MAC-E-Filter principle therefore poses a non-trivial challenge.

Simulations of the transmission properties of the spectrometer are essential in understanding the flaws and weaknesses in a design. Here they lead to a new electrode setup, that offers a better screening and thus more homogeneous fields going from $\Delta U \approx 150$ V in the old setup to a potential inhomogeneity of only $\Delta U \approx 5$ V in the final setup. For an improvement of also the magnetic field shape in the analysing plane an air-coil was added to the system.

Transmission function measurements have been performed for the 17.8 keV electrons at two different magnetic field settings with 5 A and 15 A coil currents. The resulting spectra exhibit a constant offset caused by background electrons ejected from the electrode system due to soft x-rays emitted from the ^{83}Rb/^{83m}Kr source implemented in the setup. Taking this background into account, a simple fit of the theoretical transmission function to the data gives a qualitative agreement and correct numbers for the ratios of the magnetic field strength in the source and analysing plane.
Deviations from the theoretical curve occur at the upper edge of the transmission function. These deviations are caused on the one hand by energy losses of the conversion electrons when leaving the material of the implanted HOPG source. The additional oscillation on the transmission plateau is most probably caused by the limited size of the active detector area and the phase of the cyclotron motion of the electrons, which is modulated by the retardation voltage. Depending on this phase, the electrons have a higher or lower chance hitting the detector cap and be lost for detection. A similar effect has been observed and analysed in the PhD thesis of M. Zacher who performed simulations and measurements for a photo-electron calibration source for KATRIN [Zac14].

To develop a suitable fit model taking all these effects into account would require reliable data on the actual energy losses of the conversion electrons in the implanted sources used and additional simulations investigating the effects of the cyclotron phase on the

transmission function. These investigations were outside the scope of this thesis but could be studied in a future effort.

8 Appendix

8.1 Bibliography

References

[Ago+13] M. Agostini et al. *Results on neutrinoless double beta decay of* 76Ge *from GERDA Phase I.* Phys. Rev. Lett., 111, 2013.

[AJG+05] Ahrens, James, Geveci, Berk, Law, and Charles. *Paraview: An End-User Tool for Large Data Visualization, Visualization Handbook.* Elsevier, 2005.

[Ase+11] V. N. Aseev et al. *An upper limit on electron antineutrino mass from Troitsk experiment.* Phys. Rev., 84, 2011.

[Beh12] J. D. Behrens. *Simulations of stored electrons in the Penning trap between the KATRIN spectrometers.* Diploma thesis, Westfälische-Wilhelms-Universität - Institut für Kernphysik, 2012.

[Beh16] J. D. Behrens. *Design and comissioning of a monoenergetic photoelectron source and active background reduction by magnetic pulse at the KATRIN experiment.* PhD thesis, Westfälische-Wilhelms-Universität - Institut für Kernphysik, 2016.

[Gro15] Stephan Groh. *Modelling of the response function and measurement of transmission properties of the KATRIN experiment.* PhD thesis, Karlsruher Institut für Experimentelle Kernphysik - Karlsruher Institut für Technologie, 2015.

[Hil11] Björn Hillen. *Untersuchung von Methoden zur Unterdrückung des Spektrometeruntergrunds beim KATRIN Experiment.* PhD thesis, Westfälische-Wilhelms-Universität - Institut für Kernphysik, 2011.

[Kat06] KAT Komitee für Astroteilchenphysik. *Kosmische Spurensuche: Astroteilchenphysik in Deutschland, Ein Forschungsgebiet im Aufbruch.* Forschungszentrum Karlsruhe in der Helmholtz-Gemeinschaft, 2006.

[Kra+13] C. Kraus et al. *Final Results from phase II of the Mainz Neutrino Mass Search in Tritium β Decay.* Eur. Phys. J., 40:447-468, 2005.

[RC59] Reines.R and Cowan.C.L. *Free Antineutrino Absorption Cross Section. First Measurement of the Free Antineutrino Absorption Cross Section by Protons.* Phys.Rev., 113:273, 1959.

[RS12] S. Riemer-Sørensen. *WiggleZ Dark Energy Survey, Cosmological neutrino mass constraint from blue high-redshift galaxies. Phys.Rev.*, D85, 2012.

[Sch90] M. Schrader *Rauschoptimierung eines ladungsempfindlichen Vorverstärkers für Halbleiterdetektoren und digitale Filterung des analogen Ausgangssignals.* Diploma thesis, Johannes Gutenberg Universität Mainz - Institut für Physik, 1990.

[Sle15] Martin Slezak. *Monitoring of the energy scale in the KATRIN neutrino experiment.* PhD thesis, Charles University in Prague - Faculty of Mathematics and Physics, 2015.

[SK98] The Super-Kamiokande Collaboration. *Evidence for oscillation of atmospheric neutrinos.* Phys. Rev. Lett., 81:1562, 1998.

[Tro+17] Nikolaus Trost, Martin Babutzka, John P. Barrett, Jan Behrens, Nicholas Buzinsky, Thomas Corona, Sanshiro Enomoto, Moritz Erhard, Joseph A. A. Formaggio, Ferenc Glück Glück, Fabian Harms, Florian Heizmann, Daniel Hilk, Wolfgang Käfer, Marco Kleesiek, Benjamin Leiber, Susanne Mertens, Noah S. Oblath, Pascal Renschler, Johannes Schwarz, Penny L. Slocum, Nancy Wandkowsky, Kevin Wierman, Daniel Furse, Stefan Groh, and Michael Zacher. *Kassiopeia: a modern, extensible C++ particle tracking package.* New Journal of Physics, 19, 2017.

[Woj] M. Wojdyr *Fityk : a general-purpose peak fitting program.* J. Appl. Cryst., 43:1126-1128, 2010.

[Zac14] Michael Zacher. *High-field electrodes design and an angular-selective photoelectron source for the KATRIN spectrometers.* PhD thesis, Westfälische-Wilhelms-Universität - Institut für Kernphysik, 2014.

8.2 Kassiopeia config xml-files

8.2.1 Katrino Geometry

```
<geometry>
<!-- world -->

<cylinder_space name="world_space" z1="-2." z2="2." r="2."/>

<!-- target space (small space in front of detector and source surface
   for navigation purposes) -->

<cylinder_tube_space name="target_detector_space" z1="-0.1185" z2="
   -0.118" r1="1.9e-3" r2="5.5e-3"/>

<!-- mask spaces -->

<cylinder_space name="mask_space" z1="{[solenoid_distanceFromCenter
   ]-0.0269+0.005}"
z2="{[solenoid_distanceFromCenter]-0.0269-0.005}" r="6.e-3"/>

<!-- magnet -->

<tag name="magnet_tag">
  <tag name="airCoil">
    <cylinder_tube_space name="airCoil_space" z1="{-[airCoilLength]/2}"
       z2="{[airCoilLength]/2}" r1="0.157"
    r2="0.225" longitudinal_mesh_count="256" longitudinal_mesh_power="
       1.5" radial_mesh_count="32"
    radial_mesh_power="1.5" axial_mesh_count="128" />
  </tag>
        <cylinder_tube_space name="solenoid_space" z1="-2.345e-2" z2="
           2.345e-2" r1="1.99999999e-2"
    r2="2.0e-2" longitudinal_mesh_count="32" longitudinal_mesh_power="2.
       " radial_mesh_count="30"
    radial_mesh_power="1.5" axial_mesh_count="32" />
</tag>

<tag name="electrode_tag">

<tag name="ring_electrode_tag">
<!-- ringelectrode -->
```

```
<cylinder_surface name="electrode_ring_surface" z1="{-[
    ringElectrode_length]/2.}" z2="{[ringElectrode_length]/2.}"
r="[ringElectrode_radius]" longitudinal_mesh_count="400"
    longitudinal_mesh_power="1.2" axial_mesh_count="64"/>

<tag name="cut_cone_tag">
  <cut_cone_surface name="ring_electrode_cut_cone_surface" z1="{[
      cut_cone_length]/2}" r1="6.0e-2"
  z2="{-[cut_cone_length]/2}" r2="{6.0e-2-[cut_cone_radius]}"
      longitudinal_mesh_count="40"
  longitudinal_mesh_power="1.2" axial_mesh_count="32"/>
</tag>

<rotated_arc_segment_surface name="electrode_ring_rotated_arc_segment"
    rotated_mesh_count="128">
  <arc_segment x1="0.0" y1="{[ringElectrode_radius]-[cut_cone_radius
      ]+0.9e-2}" x2="-0.002" y2="{[ringElectrode_radius]-[cut_cone_radius
      ]+0.9e-2}" radius="0.001"
  right="true" short="true" arc_mesh_count="64"/>
</rotated_arc_segment_surface>

<torus_surface name="electrode_ring_inner_rotated_arc_segment" z="0." r=
    "{[ringElectrode_radius]-[cut_cone_radius]+(0.007/sqrt([
    cut_cone_length]**2+[cut_cone_radius]**2))*[cut_cone_length]}" radius
    ="0.007" toroidal_mesh_count="64"
axial_mesh_count="64"/>

<annulus_surface name="electrode_ring_annulus_surface" z="0.0" r1="{[
    ringElectrode_radius]-[cut_cone_radius]}" r2="{[ringElectrode_radius
    ]-[cut_cone_radius]+0.9e-2}"
radial_mesh_count="6" radial_mesh_power="1.5" axial_mesh_count="64"/>

<tag name="central_electrode_tag">
  <!-- central electrode disk -->

  <cylinder_surface name="central_disk_surface" z1="-1.5e-3" z2="1.5e-3"
      r="1.0e-2" longitudinal_mesh_count="8"
      longitudinal_mesh_power="2."
  axial_mesh_count="16"/>

    <disk_surface name="central_disk_disk_surface" z="0." r="1.e-2"
       radial_mesh_count="14" radial_mesh_power="1.5"
```

```
                                axial_mesh_count="16"/>

    <!-- electrode staff for central disk -->
    <extruded_poly_loop_surface name="
       central_disk_staff_extruded_surface" zmin="-0.75e-3" zmax="0.75e
       -3"
    extruded_mesh_count="4" extruded_mesh_power="1.2">
  <poly_loop>
    <start_point x="9.88691e-3" y="0.75e-3"/>
    <next_arc x="9.88691e-3" y="-0.75e-3" radius="1.0e-2" right="false"
       short="true" arc_mesh_count="8"/>
    <next_line x="59.9e-3" y="-0.75e-3" line_mesh_count="4"
       line_mesh_power="1.5"/>
    <next_arc x="59.9e-3" y="0.75e-3" radius="6.0e-2" right="false"
       short="true" arc_mesh_count="8"/>
    <last_line line_mesh_count="4" line_mesh_power="1.5"/>
  </poly_loop>
    </extruded_poly_loop_surface>
    <flattened_poly_loop_surface name="central_disk_staff_surface" z="0.
       " flattened_mesh_count="4"
    flattened_mesh_power="1.2">
  <poly_loop>
    <start_point x="9.88691e-3" y="0.75e-3"/>
    <next_arc x="9.88691e-3" y="-0.75e-3" radius="1.0e-2" right="false"
       short="true" arc_mesh_count="8"/>
    <next_line x="59.9e-3" y="-0.75e-3" line_mesh_count="4"
       line_mesh_power="1.2"/>
    <next_arc x="59.9e-3" y="0.75e-3" radius="6.0e-2" right="false"
       short="true" arc_mesh_count="8"/>
    <last_line line_mesh_count="4" line_mesh_power="1.5"/>
    <!-- actual outer stop point of the line is 59.99531514252889e-3!!
       -->
  </poly_loop>
    </flattened_poly_loop_surface>
</tag>
</tag>

<!-- magnet + cap electrode (0V surfaces) -->
<tag name="magnet_electrode_tag">

<!-- chamber -->
```

```
<tag name="chamber_tag">
  <cylinder_surface name="oven_surface" z1="-{[
     solenoid_distanceFromCenter]+0.02}" z2="{-([
     solenoid_distanceFromCenter]+0.02-0.6)}" r="1.0e-1"
     longitudinal_mesh_count="64" longitudinal_mesh_power="1.2"
      axial_mesh_count="16"/>
  <disk_surface name="oven_downstream_lid" z="-{[
     solenoid_distanceFromCenter]+0.02}" r="1.0e-1" radial_mesh_count=
     "32" radial_mesh_power="1.5"
  axial_mesh_count="16"/>
  <disk_surface name="oven_upstream_lid" z="{-([
     solenoid_distanceFromCenter]+0.02-0.6)}" r="1.0e-1"
     radial_mesh_count="32" radial_mesh_power="1.5" axial_mesh_count="
     16"/>
</tag>

<!-- caps -->
<tag name="cap">
  <!-- source cap-->
  <tag name="source_cap">
  <cylinder_surface name="source_cap_outer_cylinder_surface" z1="0" z2
     ="0.1e-3" r="4.5e-3" longitudinal_mesh_count="6"
  longitudinal_mesh_power="1.5" axial_mesh_count="16"/>
  <cylinder_surface name="source_cap_inner_cylinder_surface" z1="0" z2
     ="0.1e-3" r="2.3e-3" longitudinal_mesh_count="6"
  longitudinal_mesh_power="1.5" axial_mesh_count="16"/>
  <annulus_surface name="source_cap_annulus_surface" z="0." r1="4.5e-3
     " r2="1.3e-2" radial_mesh_count="8" radial_mesh_power="1.5"
     axial_mesh_count="16"/>
  <disk_surface name="source_cap_disk_surface" z="0." r="2.3e-3"
     radial_mesh_count="10" radial_mesh_power="1.5"
  axial_mesh_count="16"/>

  <rotated_arc_segment_surface name="source_cap_rotated_arc_segment"
     rotated_mesh_count="64">
    <arc_segment x1="0.0035" y1="0.02" x2="-0.0035" y2="0.013" radius=
       "0.007" right="true" short="true"
    arc_mesh_count="64"/>
  </rotated_arc_segment_surface>

  <extruded_poly_loop_surface name="source_cap_staff_extruded_surface"
      zmin="-0.1e-3" zmax="0."
```

```
    extruded_mesh_count="4" extruded_mesh_power="1.2">
      <poly_loop>
        <start_point x="2.28637267e-3" y="0.25e-3"/><!-- 2.28637267 -->
        <next_arc x="2.28637267e-3" y="-0.25e-3" radius="2.3e-3" right="
           false" short="true" arc_mesh_count="2"/>
        <next_line x="4.49305019e-3" y="-0.25e-3" line_mesh_count="4"
           line_mesh_power="1.5"/><!-- 4.49305019 -->
        <next_arc x="4.49305019e-3" y="0.25e-3" radius="4.5e-3" right="
           false" short="true" arc_mesh_count="2"/>
        <last_line line_mesh_count="4" line_mesh_power="1.5"/>
      </poly_loop>
    </extruded_poly_loop_surface>
    <flattened_poly_loop_surface name="source_cap_staff_surface" z="0."
       flattened_mesh_count="4"
        flattened_mesh_power="1.2">
      <poly_loop>
        <start_point x="2.28637267e-3" y="0.25e-3"/>
        <next_arc x="2.28637267e-3" y="-0.25e-3" radius="2.3e-3" right="
           false" short="true" arc_mesh_count="2"/>
        <next_line x="4.49305019e-3" y="-0.25e-3" line_mesh_count="4"
           line_mesh_power="1.5"/>
        <next_arc x="4.49305019e-3" y="0.25e-3" radius="4.5e-3" right="
           false" short="true" arc_mesh_count="2"/>
        <last_line line_mesh_count="4" line_mesh_power="1.5"/>
      </poly_loop>
        </flattened_poly_loop_surface>
    </tag>
    <tag name="detector_cap">
    <!-- detector cap -->
      <cylinder_surface name="detector_cap_outer_cylinder_surface" z1="
         0." z2="0.1e-3" r="9.5e-3" longitudinal_mesh_count="6"
      longitudinal_mesh_power="1.5" axial_mesh_count="24"/>

      <cylinder_surface name="detector_cap_inner_cylinder_surface" z1="
         0." z2="0.1e-3" r="1.9e-3" longitudinal_mesh_count="6"
      longitudinal_mesh_power="1.5" axial_mesh_count="24"/>

      <annulus_surface name="detector_cap_annulus_surface" z="0." r1="
         9.5e-3" r2="1.3e-2" radial_mesh_count="8" radial_mesh_power="
         1.5" axial_mesh_count="24"/>

      <disk_surface name="detector_cap_disk_surface" z="0." r="1.9e-3"
```

```
      radial_mesh_count="10" radial_mesh_power="1.5"
    axial_mesh_count="16"/>

    <rotated_arc_segment_surface name="
      detector_cap_rotated_arc_segment" rotated_mesh_count="16">
      <arc_segment x1="0.0035" y1="0.02" x2="-0.0035" y2="0.013"
        radius="0.007" right="true" short="true"
      arc_mesh_count="16"/>
    </rotated_arc_segment_surface>

    <extruded_poly_loop_surface name="
      detector_cap_staff_extruded_surface" zmin="-0.1e-3" zmax="0."
    extruded_mesh_count="4" extruded_mesh_power="1.2">
    <poly_loop>
      <start_point x="1.8834808e-3" y="0.25e-3"/>
      <next_arc x="1.8834808e-3" y="-0.25e-3" radius="1.9e-3" right="
        false" short="true" arc_mesh_count="2"/>
      <next_line x="9.49967e-3" y="-0.25e-3" line_mesh_count="8"
        line_mesh_power="1.5"/>
      <next_arc x="9.49967e-3" y="0.25e-3" radius="9.5e-3" right="
        false" short="true" arc_mesh_count="2"/>
      <last_line line_mesh_count="8" line_mesh_power="1.5"/>
    </poly_loop>
    </extruded_poly_loop_surface>
      <flattened_poly_loop_surface name="detector_cap_staff_surface" z
        ="0." flattened_mesh_count="4"
      flattened_mesh_power="1.2">
    <poly_loop>
      <start_point x="1.8834808e-3" y="0.25e-3"/>
      <next_arc x="1.8834808e-3" y="-0.25e-3" radius="2.3e-3" right="
        false" short="true" arc_mesh_count="2"/>
      <next_line x="9.49967e-3" y="-0.25e-3" line_mesh_count="8"
        line_mesh_power="1.5"/>
      <next_arc x="9.49967e-3" y="0.25e-3" radius="9.5e-3" right="
        false" short="true" arc_mesh_count="2"/>
      <last_line line_mesh_count="8" line_mesh_power="1.5"/>
    </poly_loop>
      </flattened_poly_loop_surface>
  </tag>
  </tag>
  <!-- magnet electrode -->
  <cylinder_surface name="solenoid_surface_inner" z1="-2.e-2" z2="2.e
```

```
        -2" r="3.0e-3" longitudinal_mesh_count="6"
        longitudinal_mesh_power="1.5" axial_mesh_count="10"/>

    <cylinder_surface name="solenoid_surface_outer" z1="-2.e-2" z2="2.e
        -2" r="2.0e-2" longitudinal_mesh_count="10"
        longitudinal_mesh_power="1.5"
    axial_mesh_count="10"/>

    <annulus_surface name="solenoid_surface_annulus" z="0." r1="3.e-3"
        r2="2.e-2" radial_mesh_count="8" radial_mesh_power="1.2"
    axial_mesh_count="10"/>

    <disk_surface name="solenoid_surface_disk" z="0." r="3.e-3"
        radial_mesh_count="3" radial_mesh_power="1.2" axial_mesh_count="
        10"/>

    <annulus_surface name="source_surface" z="0." r1="2.3e-3" r2="4.5e-3
        " radial_mesh_count="15" radial_mesh_power="1.5"
    axial_mesh_count="64"/>
  </tag>

<annulus_surface name="detector_surface_electrode" z="0." r1="1.9e-3" r2
    ="9.5e-3" radial_mesh_count="12" radial_mesh_power="1.25"
    axial_mesh_count="16"/><!-- radial_mesh_count="35" axial_mesh_count="
    96" -->

    <tag name="detector_tag">
      <!-- surface of photodiode -->
  <tag name="detector_surface">
      <flattened_poly_loop_surface name="detector_surface" z="0."
        flattened_mesh_count="10"
  flattened_mesh_power="4.">
          <poly_loop>
                <start_point x="4.5e-3" y="4.5e-3"/>
                <next_line x="-4.5e-3" y="4.5e-3" line_mesh_count="40"
                    line_mesh_power="1.2"/>
                <next_line x="-4.5e-3" y="-4.5e-3" line_mesh_count="40"
                    line_mesh_power="1.2"/>
                <next_line x="4.5e-3" y="-4.5e-3" line_mesh_count="40"
                    line_mesh_power="1.2"/>
          <last_line line_mesh_count="40" line_mesh_power="1.2"/>
          </poly_loop>
```

```
    </flattened_poly_loop_surface>
</tag>
 </tag>
 </tag>

  <!-- assembly -->

  <space name="Katrino_assembly">
<!-- oven -->
<surface name="oven_cylind" node="oven_surface"/>
<surface name="oven_downstream_lid" node="oven_downstream_lid"/>
<surface name="oven_upstream_lid" node="oven_upstream_lid"/>
<!-- ring electrode -->
  <surface name="ring_electrode" node="electrode_ring_surface"/>
<!-- up -->
<surface name="electrode_ring_inner_rotated_arc_segment_up" node="
   electrode_ring_inner_rotated_arc_segment">
  <transformation displacement="0 0 {[cut_cone_length]+[
     ringElectrode_length]/2+(0.007/sqrt([cut_cone_length]**2+[
     cut_cone_radius]**2))*[cut_cone_radius]}"/>
</surface>
<surface name="ring_electrode_cut_cone_surface_up" node="
   ring_electrode_cut_cone_surface">
  <transformation displacement="0. 0. {([ringElectrode_length]+[
     cut_cone_length])/2.}"
  rotation_euler="0 180 0"/>
</surface>
<!-- down -->
<surface name="electrode_ring_inner_rotated_arc_segment_down" node="
   electrode_ring_inner_rotated_arc_segment">
  <transformation displacement="0 0 -{[cut_cone_length]+[
     ringElectrode_length]/2+(0.007/sqrt([cut_cone_length]**2+[
     cut_cone_radius]**2))*[cut_cone_radius]}"/>
</surface>
<surface name="ring_electrode_cut_cone_surface_down" node="
   ring_electrode_cut_cone_surface">
    <transformation displacement="0. 0. -{([ringElectrode_length]+[
       cut_cone_length])/2.}"/>
</surface>
  <!-- central disk electrode-->
  <surface name="central_disk_electrode" node="central_disk_surface"/>
  <surface name="central_disk_disk_electrode_down" node="
```

```
      central_disk_disk_surface">
    <transformation displacement="0. 0. -1.5e-3"/>
  </surface>
      <surface name="central_disk_disk_electrode_up" node="
        central_disk_disk_surface">
    <transformation displacement="0. 0. 1.5e-3"/>
  </surface>
  <!-- magnet cap-->
  <!-- source cap -->
  <surface name="source_cap_rotated_arc" node="
     source_cap_rotated_arc_segment">
    <transformation displacement="0. 0. {[solenoid_distanceFromCenter
        ]-0.0235}"/>
  </surface>
  <surface name="source_cap_outer_cylinder" node="
     source_cap_outer_cylinder_surface">
    <transformation displacement="0. 0. {[solenoid_distanceFromCenter
        ]-0.027}"/>
  </surface>
  <surface name="source_cap_inner_cylinder" node="
     source_cap_inner_cylinder_surface">
    <transformation displacement="0. 0. {[solenoid_distanceFromCenter
        ]-0.027}"/>
  </surface>
  <surface name="source_cap_annulus" node="source_cap_annulus_surface">
    <transformation displacement="0. 0. {[solenoid_distanceFromCenter
        ]-0.027}"/>
  </surface>
  <surface name="source_cap_disk" node="source_cap_disk_surface">
    <transformation displacement="0. 0. {[solenoid_distanceFromCenter
        ]-0.027}"/>
  </surface>
  <surface name="source_surface" node="source_surface">
    <transformation displacement="0. 0.  {[solenoid_distanceFromCenter
        ]-0.0269}"/>
  </surface>
  <!-- detector cap -->
  <surface name="detector_cap_rotated_arc" node="
     detector_cap_rotated_arc_segment">
    <transformation rotation_euler="0 180 0" displacement="0. 0. {-[
        solenoid_distanceFromCenter]+0.0235}"/>
  </surface>
```

```
<surface name="detector_cap_outer_cylinder" node="
    detector_cap_outer_cylinder_surface">
  <transformation displacement="0. 0. {-[solenoid_distanceFromCenter
      ]+0.0269}"/>
</surface>
<surface name="detector_cap_inner_cylinder" node="
    detector_cap_inner_cylinder_surface">
  <transformation displacement="0. 0. {-[solenoid_distanceFromCenter
      ]+0.0269}"/>
</surface>
<surface name="detector_cap_disk" node="detector_cap_disk_surface">
  <transformation displacement="0. 0.{-[solenoid_distanceFromCenter
      ]+0.0269}"/>
</surface>
<surface name="detector_cap_annulus" node="
    detector_cap_annulus_surface">
  <transformation displacement="0. 0. {-[solenoid_distanceFromCenter
      ]+0.0269}"/>
</surface>
<surface name="detector_surface_electrode" node="
    detector_surface_electrode">
  <transformation displacement="0. 0. {-[solenoid_distanceFromCenter
      ]+0.0269}"/>
</surface>
<surface name="detector_surface" node="detector_surface">
  <transformation displacement="0. 0. {-[solenoid_distanceFromCenter
      ]+0.0269+[detector_displacement]}"/>
</surface>
<if condition="{!([detector_displacement] eq 0.)}">
  <surface name="detector_backendSurface" node="
      detector_backendSurface">
    <transformation displacement="0. 0. {-[solenoid_distanceFromCenter
        ]+0.0269+[detector_displacement]-0.0005}"/>
  </surface>
  <surface name="detector_sideSurface_up" node="detector_sideSurface">
    <transformation rotation_euler="0 90 0"/>
    <transformation displacement="0. 4.5e-3 {-[
        solenoid_distanceFromCenter]+0.0269+[detector_displacement
        ]-0.00025}"/>
  </surface>
  <surface name="detector_sideSurface_down" node="detector_sideSurface
      ">
```

```
      <transformation rotation_euler="0 90 0"/>
      <transformation displacement="0. -4.5e-3 {-[
         solenoid_distanceFromCenter]+0.0269+[detector_displacement
         ]-0.00025}"/>
    </surface>
    <surface name="detector_sideSurface_right" node="
       detector_sideSurface">
      <transformation rotation_euler="90 90 0"/>
      <transformation displacement="4.5e-3 0. {-[
         solenoid_distanceFromCenter]+0.0269+[detector_displacement
         ]-0.00025}"/>
    </surface>
    <surface name="detector_sideSurface_left" node="detector_sideSurface
       ">
      <transformation rotation_euler="90 90 0"/>
      <transformation displacement="-4.5e-3 0. {-[
         solenoid_distanceFromCenter]+0.0269+[detector_displacement
         ]-0.00025}"/>
    </surface>
  </if>
  <!-- downstream solenoid surfaces-->
  <surface name="downstream_solenoid_surface_in" node="
     solenoid_surface_inner">
    <transformation displacement="0. 0. -[solenoid_distanceFromCenter]"/
       >
  </surface>
  <surface name="downstream_solenoid_surface_out" node="
     solenoid_surface_outer">
    <transformation displacement="0. 0. -[solenoid_distanceFromCenter]"/
       >
  </surface>
  <surface name="downstream_solenoid_surface_annulus" node="
     solenoid_surface_annulus">
    <transformation displacement="0. 0. {-[solenoid_distanceFromCenter
       ]-0.02}"/>
  </surface>
  <surface name="downstream_solenoid_surface_disk" node="
     solenoid_surface_disk">
    <transformation displacement="0. 0. {-[solenoid_distanceFromCenter
       ]+0.02}"/>
  </surface>
  <!-- upstream solenoid surfaces-->
```

```
<surface name="upstream_solenoid_surface_in" node="
    solenoid_surface_inner">
  <transformation displacement="0. 0. [solenoid_distanceFromCenter]"/>
</surface>
<surface name="upstream_solenoid_surface_out" node="
    solenoid_surface_outer">
  <transformation displacement="0. 0. [solenoid_distanceFromCenter]"/>
</surface>
<surface name="upstream_solenoid_surface_disk" node="
    solenoid_surface_disk">
  <transformation displacement="0. 0. {[solenoid_distanceFromCenter
      ]-0.02}"/>
</surface>
<surface name="upstream_solenoid_surface_annulus" node="
    solenoid_surface_annulus">
  <transformation displacement="0. 0. {[solenoid_distanceFromCenter
      ]+0.02}"/>
</surface>
<!-- downstram solenoid space-->
  <space name="downstream_solenoid" node="solenoid_space">
    <transformation displacement="0. 0. -[solenoid_distanceFromCenter]
        "/>
  </space>
  <!-- upstream solenoid space -->
  <space name="upstream_solenoid" node="solenoid_space">
    <transformation displacement="0. 0. [solenoid_distanceFromCenter]"
        />
  </space>
<!-- Aircoil -->
<space name="airCoil" node="airCoil_space"/>
<!-- mask space -->
<space name="mask_space" node="mask_space">
  <transformation displacement="0. 3.4e-3 0."/>
</space>
  </space>

  <space name="world" node="world_space">
      <space name="Katrino" tree="Katrino_assembly"/>
  </space>

  <!--  bem -->
```

```
    <electrostatic_dirichlet name="ring_electrode" surfaces="world/
       Katrino/@ring_electrode_tag" value="[electrodeVoltage]"/>
    <electrostatic_dirichlet name="magnet_electrode" surfaces="world/
       Katrino/@magnet_electrode_tag" value="0."/>
    <electrostatic_dirichlet name="detector_cap_electrode" surfaces="
       world/Katrino/detector_surface_electrode" value="0."/>

    <!-- electromagnets -->

    <electromagnet name="electromagnet_solenoid" spaces="world/Katrino/
       downstream_solenoid" current="48682.8270"/>
    <electromagnet name="electromagnet_solenoid" spaces="world/Katrino/
       upstream_solenoid" current="48682.8270"/>
    <electromagnet name="electromagnet_airCoil" spaces="world/Katrino/
       airCoil" current="{150*[airCoilCurrent]}"/>

    <!-- mesh -->

    <axial_mesh name="axial_mesh_electrode" surfaces="world/Katrino/
       @electrode_tag"/>
    <mesh name="mesh_electrode" surfaces="world/Katrino/@electrode_tag"/
       >

</geometry>
```

8.2.2 Config

```
<include name=".../[GeoXml]"/>

<kassiopeia>

<!-- magnetic field -->

<ksfield_electromagnet name="field_magnets" directory="[KEMField_path]"
   file="[magnetFilename]_current[airCoilCurrent].kbd" system="world/
   Katrino" spaces="world/Katrino/@magnet_tag">

 <zonal_harmonic_field_solver number_of_bifurcations="-1"
    convergence_ratio=".99" convergence_parameter="1.e-15"
 proximity_to_sourcepoint="1.e-12" number_of_central_coefficients="500"
    use_fractional_central_sourcepoint_spacing="true"
 central_sourcepoint_fractional_distance="1.e-2"
```

```
    central_sourcepoint_spacing="1.e-3"
 number_of_remote_coefficients="200" />

</ksfield_electromagnet>

<!-- electric field -->

<ksfield_electrostatic name="field_electrostatic" directory="[
   KEMField_path]" file="[electrodeFilename].kbd"
system="world/Katrino" surfaces="world/Katrino/@electrode_tag" symmetry=
   "axial">

  <viewer file="[KEMField_path]/[electrodeFilename].vtp" view="false"
     save="true"
  preprocessing="false" postprocessing="true"/>

  <!-- cache matrix elements uses a lot of memory, should be turned to
     false in non axial field computation-->
  <robin_hood_bem_solver tolerance="1.e-10" check_sub_interval="100"
     display_interval="1"
  cache_matrix_elements="true" use_vtk="true"/>

  <zonal_harmonic_field_solver number_of_bifurcations="-1"
     convergence_ratio=".99" convergence_parameter="1.e-15"
  proximity_to_sourcepoint="1.e-12" number_of_central_coefficients="500"
      use_fractional_central_sourcepoint_spacing="true"
  central_sourcepoint_fractional_distance="1.e-2"
     central_sourcepoint_spacing="1.e-3"
  number_of_remote_coefficients="200"/>
</ksfield_electrostatic>

<!-- generator for equally distributed starting position, with gaussian
   energy width -->

<ksgen_generator_composite name="eq_positioning" pid="11">
  <!--time-->
  <time_composite>
    <time_fix value="0."/>
  </time_composite>
  <!--energy-->
  <energy_composite>
    <energy_gauss value_mean="30472.3" value_sigma="1.19"/>
```

```
  </energy_composite>
  <!--position-->
  <position_mask spaces_allowed="world/Katrino/mask_space" max_retries="
     100">
    <position_mesh_surface_random surfaces="world/Katrino/source_surface
       "/>
  </position_mask>
  <position_surface_adjustment_step length="-1e-10"/>
  <!--direction-->
  <direction_surface_composite surfaces="world/Katrino/source_surface"
     outside="false">
    <theta_spherical angle_min="0." angle_max="90."/>
    <phi_uniform value_min="0." value_max="360."/>
  </direction_surface_composite>
</ksgen_generator_composite>

<!--  adiabatic trajectory -->

 <kstraj_trajectory_adiabatic name="trajectory_adiabatic">
     <integrator_rk8 name="integrator_rk8"/>
     <term_propagation name="term_propagation"/>
     <term_gyration name="term_gyration"/>
     <term_drift name="term_drift"/>
     <term_synchrotron name="term_synchrotron"/>
     <control_cyclotron name="control_cyclotron" fraction="{1./8.}"/>
 </kstraj_trajectory_adiabatic>

<!-- space navigators -->

<ksnav_space name="nav_space" enter_split="false" exit_split="false"/>

<!-- surface navigators -->

<ksnav_surface name="nav_surface" transmission_split="false"
   reflection_split="false"/>

<!-- terminators -->

 <ksterm_death name="term_source"/>
 <ksterm_death name="term_detector"/>
 <ksterm_death name="term_cap_src"/>
 <ksterm_death name="term_cap_det"/>
```

```
 <ksterm_death name="term_central_electrode"/>
 <ksterm_death name="term_cut_cone"/>
 <ksterm_death name="term_world"/>
 <ksterm_max_steps name="term_max_steps" steps="10000"/>
 <ksterm_max_r name="term_max_r" r="0.06001"/>
 <ksterm_min_z name="term_min_z" z="{-[solenoid_distanceFromCenter
    ]+0.0269+[detector_displacement]}"/>
 <ksterm_trapped name="term_trapped" max_turns="4"/>

<!-- writers -->

 <kswrite_root name="write_root" path="[output_path]" base="[rootBase].
    root"/>
 <kswrite_vtk name="write_vtk" path="[output_path]" base="[vtkBase]"/>

<!-- output -->

 <ks_component_member name="component_step_final_particle" field="
    final_particle" parent="step"/>
 <ks_component_member name="electric_potential" field="
    electric_potential" parent="component_step_final_particle"/>
 <ks_component_member name="kinetic_energy" field="kinetic_energy_ev"
    parent="component_step_final_particle"/>
 <ks_component_member name="polar_angle_to_b" field="polar_angle_to_b"
    parent="component_step_final_particle"/>

 <ks_component_group name="component_step_world">
  <component_member name="step_id" field="step_id" parent="step"/>
        <component_member name="time" field="time" parent="
           component_step_final_particle"/>
        <component_member name="position" field="position" parent="
           component_step_final_particle"/>
        <component_member name="momentum" field="momentum" parent="
           component_step_final_particle"/>
        <component_member name="magnetic_field" field="magnetic_field"
           parent="component_step_final_particle"/>
        <component_member name="electric_field" field="electric_field"
           parent="component_step_final_particle"/>
        <component_member name="electric_potential" field="
           electric_potential" parent="component_step_final_particle"/>
        <component_member name="kinetic_energy" field="kinetic_energy_ev
           " parent="component_step_final_particle"/>
```

```
        <component_member name="polar_angle_to_b" field="
           polar_angle_to_b" parent="component_step_final_particle"/>
</ks_component_group>

<ks_component_member name="magnetic_field" field="magnetic_field"
   parent="component_step_final_particle"/>
<ks_component_member name="magnetic_field_z" field="z" parent="
   magnetic_field"/>
<ks_component_member name="magnetic_field_y" field="y" parent="
   magnetic_field"/>
<ks_component_member name="magnetic_field_x" field="x" parent="
   magnetic_field"/>

<ks_component_member name="output_track_initial_particle" field="
   initial_particle" parent="track"/>
<ks_component_member name="output_track_final_particle" field="
   final_particle" parent="track"/>
<ks_component_group name="component_track_world">
 <component_member name="track_id" field="track_id" parent="track"/>
 <component_member name="creator_name" field="creator_name" parent="
    track"/>
 <component_member name="terminator_name" field="terminator_name"
    parent="track"/>
 <component_member name="total_steps" field="total_steps" parent="track
    "/>
 <component_member name="initial_position" field="position" parent="
    output_track_initial_particle"/>
 <component_member name="initial_momentum" field="momentum" parent="
    output_track_initial_particle"/>
 <component_member name="initial_magnetic_field" field="magnetic_field"
     parent="output_track_initial_particle"/>
 <component_member name="initial_electric_field" field="electric_field"
     parent="output_track_initial_particle"/>
 <component_member name="initial_electric_potential" field="
    electric_potential" parent="output_track_initial_particle"/>
 <component_member name="initial_polar_angle_to_b" field="
    polar_angle_to_b" parent="output_track_initial_particle"/>
 <component_member name="final_position" field="position" parent="
    output_track_final_particle"/>
 <component_member name="final_momentum" field="momentum" parent="
    output_track_final_particle"/>
 <component_member name="final_magnetic_field" field="magnetic_field"
```

```
      parent="output_track_final_particle"/>
   <component_member name="final_electric_field" field="electric_field"
      parent="output_track_final_particle"/>
   <component_member name="final_electric_potential" field="
      electric_potential" parent="output_track_final_particle"/>
   <component_member name="final_kinetic_energy" field="kinetic_energy_ev
      " parent="output_track_final_particle"/>
 </ks_component_group>

<!-- structure -->

<ksgeo_space name="space_world" spaces="world">
   <command parent="root_terminator" field="remove_terminator" child="
      term_world"/>
   <command parent="root_terminator" field="add_terminator" child="
      term_max_steps"/>
   <command parent="root_terminator" field="add_terminator" child="
      term_max_r"/>
   <command parent="root_terminator" field="add_terminator" child="
      term_trapped"/>
   <command parent="root_terminator" field="add_terminator" child="
      term_min_z"/>
   <!-- root output -->
   <command parent="write_root" field="add_step_output" child="
      component_step_world"/>
   <command parent="write_root" field="add_step_output" child="
      component_step_Katrino"/>
   <command parent="write_root" field="add_track_output" child="
      component_track_world"/>
   <!-- geo surfaces-->
   <geo_surface name="surface_upstream_target" surfaces="world/Katrino/
      source_surface">
     <command parent="root_terminator" field="add_terminator" child="
        term_source"/>
   </geo_surface>
   <geo_surface name="surface_cap_source" surfaces="world/Katrino/
      @source_cap">
     <command parent="root_terminator" field="add_terminator" child="
        term_cap_src"/>
   </geo_surface>
   <geo_surface name="surface_cap_source" surfaces="world/Katrino/
      @detector_cap">
```

```
    <command parent="root_terminator" field="add_terminator" child="
       term_cap_det"/>
  </geo_surface>
  <geo_surface name="surface_central_electrode" surfaces="world/Katrino/
     @central_electrode_tag">
    <command parent="root_terminator" field="add_terminator" child="
       term_central_electrode"/>
  </geo_surface>
  <if condition="{!([cut_cone_length] eq 0.)}">
       <geo_surface name="surface_cut_cone" surfaces="world/Katrino/
          @cut_cone_tag">
      <command parent="root_terminator" field="add_terminator" child="
         term_cut_cone"/>
    </geo_surface>
  </if>
    </ksgeo_space>

<!-- simulation -->

 <ks_simulation run="1" seed="0" events="1000" magnetic_field="
    field_magnets"
 electric_field="field_electrostatic" space="space_world" generator="
    eq_positioning"
 trajectory="trajectory_adiabatic" space_navigator="nav_space"
    surface_navigator="nav_surface"
 terminator="term_world" writer="write_root"/>

</kassiopeia>
```

8.3 Hamamatsu Si PIN-Diode Detector Data Sheet

Si PIN photodiode
S3590 series

Large area sensors for scintillation detection

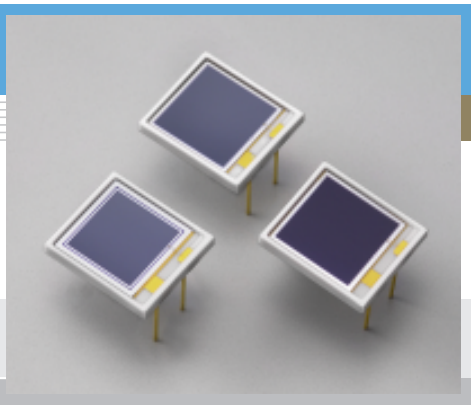

Features

- Higher sensitivity and low dark current than conventional type
- Sensitivity matching with BGO and CsI (Tl) scintillators
- High quantum efficiency: QE=85 % (λ=540 nm)
- Low capacitance
- High-speed response
- High stability
- Good energy resolution

Applications

- Scintillation detectors
- Calorimeters
- Hodoscopes
- TOF counters
- Air shower counters
- Particle detectors, etc.

■ General ratings / Absolute maximum ratings

Type No.	Window material	Active area (mm)	Absolute maximum ratings			
			Reverse voltage VR Max.	Power dissipation P (mW)	Operating temperature Topr (°C)	Storage temperature Tstg (°C)
S3590-01	Epoxy resin	10 × 10	50	100	-20 to +60	-20 to +80
S3590-02	Window-less					
S3590-05	Epoxy resin	9 × 9	150			
S3590-06	Window-less					
S3590-08	Epoxy resin	10 × 10	100			
S3590-09	Window-less					

■ Electrical and optical characteristics (Typ. Ta=25 °C, unless otherwise noted)

Type No.	Spectral response range λ (nm)	Peak sensitivity wavelength λp (nm)	Photo sensitivity S				Short circuit current Isc 100 lx (μA)	Dark current ID		Temp. coefficient of ID TCID (times/° C)	Cut-off Frequency fc (MHz)	Terminal capacitance Ct f= 1MHz (pF)	NEP VR=70 V (W/Hz$^{1/2}$)
			λ=λp (A/W)	LSO 420 nm (A/W)	BGO 480 nm (A/W)	CsI(Tl) 540 nm (A/W)		Typ. (nA)	Max. (nA)				
S3590-01	320 to 1060	920	0.58	0.19	0.26	0.31	80	1.5 *1	5 *1	1.12	35 *1	75 *1	3.9 × 10^{-14}
S3590-02			0.62	0.23	0.32	0.39							
S3590-05	320 to 1120	980	0.62	0.19	0.25	0.30	77	8 *2	30 *2		20 *2	25 *2	8.4 × 10^{-14}
S3590-06			0.64	0.23	0.32	0.39							
S3590-08	320 to 1100	960	0.66	0.20	0.30	0.36	100	2 *3	6 *3		40 *3	40 *3	3.8 × 10^{-14}
S3590-09			0.66	0.22	0.33	0.41							

*1: VR=30 V
*2: VR=100 V
*3: VR=70 V

SOLID STATE DIVISION

■ Spectral response

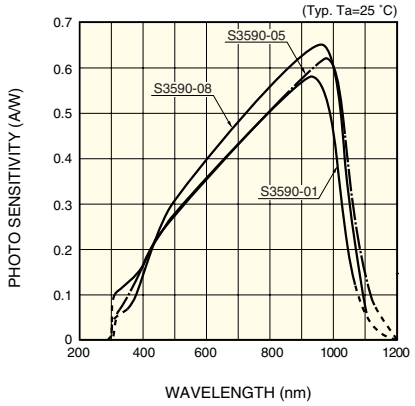

KPINB0231EA

■ Spectral response (without window)

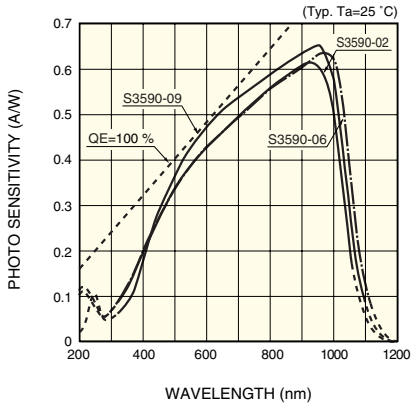

KPINB0263EA

■ Photo sensitivity temperature characteristic

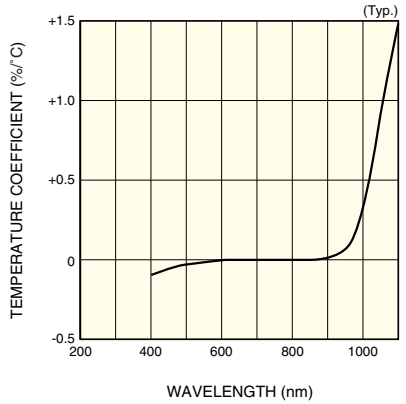

KPINB0093EC

■ Dark current vs. reverse voltage

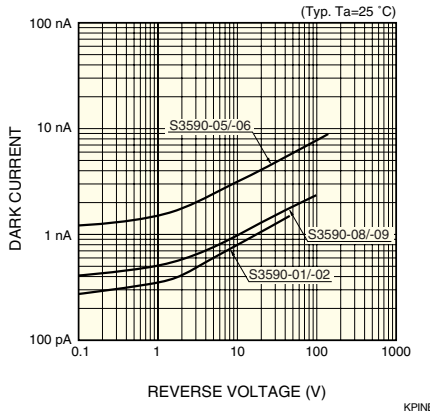

KPINB0232EB

■ Dark current vs. ambient temperature

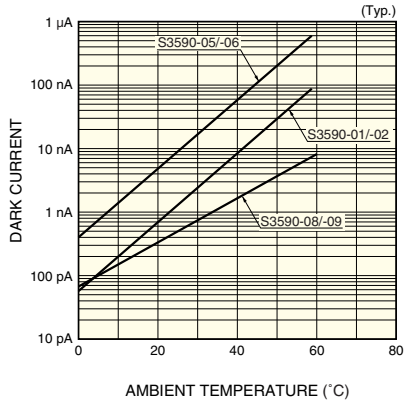

KPINB0233EB

■ Terminal capacitance vs. reverse voltage

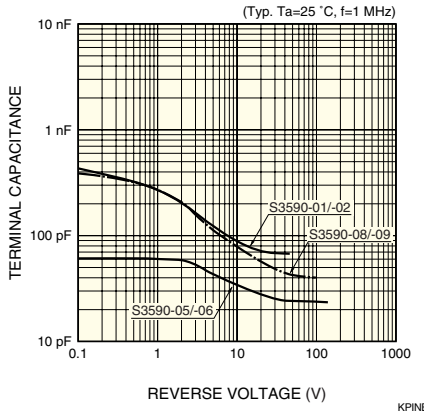

KPINB0234EB

■ Dimensional outline (unit: mm)

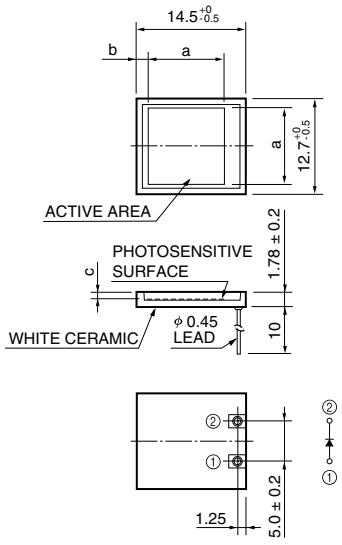

The coating resin may extend a maximum of 0.1 mm beyond the upper surface of the package.

	-01	-05	-08
a	10.0	9.0	10.0
b	1.4	1.9	1.4
c	0.8	0.5	0.7

KPINA0014EE

HAMAMATSU PHOTONICS K.K., Solid State Division
1126-1 Ichino-cho, Hamamatsu City, 435-8558 Japan, Telephone: (81) 053-434-3311, Fax: (81) 053-434-5184, http://www.hamamatsu.com
U.S.A.: Hamamatsu Corporation: 360 Foothill Road, P.O.Box 6910, Bridgewater, N.J. 08807-0910, U.S.A., Telephone: (1) 908-231-0960, Fax: (1) 908-231-1218
Germany: Hamamatsu Photonics Deutschland GmbH: Arzbergerstr. 10, D-82211 Herrsching am Ammersee, Germany, Telephone: (49) 08152-3750, Fax: (49) 08152-2658
France: Hamamatsu Photonics France S.A.R.L.: 8, Rue du Saule Trapu, Parc du Moulin de Massy, 91882 Massy Cedex, France, Telephone: 33-(1) 69 53 71 00, Fax: 33-(1) 69 53 71 10
United Kingdom: Hamamatsu Photonics UK Limited: 2 Howard Court, 10 Tewin Road, Welwyn Garden City, Hertfordshire AL7 1BW, United Kingdom, Telephone: (44) 1707-294888, Fax: (44) 1707-325777
North Europe: Hamamatsu Photonics Norden AB: Smidesvägen 12, SE-171 41 Solna, Sweden, Telephone: (46) 8-509-031-00, Fax: (46) 8-509-031-01
Italy: Hamamatsu Photonics Italia S.R.L.: Strada della Moia, 1/E, 20020 Arese, (Milano), Italy, Telephone: (39) 02-935-81-733, Fax: (39) 02-935-81-741

Cat. No. KPIN1052E03
May 2003 DN